BREAKOUT OF OBJECTS FROM UNDERCONSOLIDATED SEDIMENTS

SHIB NATH GUHA

NOTICE

The quality of this microfiche is heavily dependent upon the quality of the original thesis submitted for microfilming. Every effort has been made to ensure the highest quality of reproduction possible.

If pages are missing, contact the university which granted the degree.

Some pages may have indistinct print especially if the original pages were typed with a poor typewriter ribbon or if the university sent us a poor photocopy.

Previously copyrighted materials (journal articles, published tests, etc.) are not filmed.

Reproduction in full or in part of this film is governed by the Canadian Copyright Act, R.S.C. 1970, c. C-30. Please read the authorization forms which accompany this thesis.

THIS DISSERTATION HAS BEEN MICROFILMED EXACTLY AS RECEIVED

AVIS

La qualité de cette microfiche dépend grandement de la qualité de la thèse soumise au microfilmage. Nous avons tout fait pour assurer une qualité supérieure de reproduction.

S'il manque des pages, veuillez communiquer avec l'université qui a conféré le grade.

La qualité d'impression de certaines pages peut laisser à désirer, surtout si les pages originales ont été dactylographiées à l'aide d'un ruban usé ou si l'université nous a fait parvenir une photocopie de mauvaise qualité.

Les documents qui font déjà l'objet d'un droit d'auteur (articles de revue, examens publiés, etc.) ne sont pas microfilmés.

La reproduction, même partielle, de ce microfilm est soumise à la Loi canadienne sur le droit d'auteur, SRC 1970, c. C-30. Veuillez prendre connaissance des formules d'autorisation qui accompagnent cette thèse.

LA THÈSE A ÉTÉ MICROFILMÉE TELLE QUE NOUS L'AVONS REÇUE

BREAKOUT OF OBJECTS FROM UNDERCONSOLIDATED SEDIMENTS

by

SHIB NATH GUHA, B.Sc.(Eng.) 

A Thesis Submitted in Partial Fulfillment

of the Requirements for the Degree of

MASTER OF ENGINEERING

Faculty of Engineering and Applied Science

Memorial University of Newfoundland

September 1978

St. John's Newfoundland

ABSTRACT

There is a growing worldwide interest in the exploration, production and utilization programs for offshore oil, natural gas and other minerals. As a part of these efforts considerable interest has been directed in the last decade towards marine geotechnology. Adhesive resistance of ocean sediments is one of the important properties of marine soils which finds an application in ship salvage, refloating of exploratory platforms and relocation of marine installations such as pipelines, oil rigs, well-head manifolds, well linings and ice-soil interaction studies.

There is considerable research work reported in the literature about the adhesion and skin friction between terrestrial soils and construction materials. However, ocean floor soils differ from most terrestrial soils in their properties. Surficial ocean sediments are generally cohesive and highly underconsolidated, having very low shear strength with high liquidity index. Such soils have negligible angle of shear resistance. In the studies of interaction of such soils with embedded objects, only adhesion is of primary importance. Very little information is available at present about the adhesive resistance of these underconsolidated sediments. A closely related property is the base suction at the interface of the object base and soil, which is important

in the breakout problem

An attempt has been made in this investigation to study the adhesion and base suction during pull out tests in an artificially sedimented soil having properties comparable to those of ocean sediments. Laboratory tests were carried out to determine (a) the adhesion between the soil and objects of different surface roughness, (b) the suction at the base of prismatic objects of different base configurations during pull out, and (c) the total breakout force for fully embedded objects.

Only one type of soil was used in all the tests and the sample was prepared by mixing a pre-weighed dry soil in a known volume of water.

The adhesive resistance was found to depend on the surface roughness of the embedded objects as well as on the soil cohesion. Surface unevenness and physico-chemical action were two additional factors influencing adhesion, as observed in the tests on plexiglas and glass plate respectively.

Base suction for prismatic objects was found to be a function of the depth to breadth ration (D/B) of the object. It is higher for higher D/B values. Base configurations do not appear to have any significant influence on the base suction values.

A fairly good correlation was found between the

breakout force determined from the experiments and that estimated analytically.

Pull out tests conducted with fresh water ice sheets indicate that the adhesion - cohesion ratio is very nearly constant in the range of soil strengths tested.

ACKNOWLEDGEMENTS

This dissertation was completed at the Faculty of Engineering and Applied Science, Memorial University of Newfoundland. The project was partially funded by a National Sciences and Engineering Research Council of Canada grant #A-3710 to Dr. T.R. Chari, the project supervisor. The writer wishes to acknowledge with thanks the receipt of a Memorial University Fellowship during the period of this study.

The writer is deeply indebted to Dr. T.R. Chari, Associate Professor of Engineering, for his constant advice and guidance in the progress of this study. A number of concepts and ideas were clarified during periodic discussion with Professor W.L. White, to whom the author is grateful. Thanks are due to Dr. R. T. Dempster, Dean of Engineering for the facilities provided. The writer wishes to express his gratitude to Dr. K. Muthukrishnaiah, Post Doctoral Fellow, for his keen interest in this work and his helpful suggestions during the preparation of the thesis.

Among the various individuals who contributed to this study, the writer wishes to acknowledge, in particular, Mr. A. Bursey for his assistance in the instrumentation, Mr. P. Robinson and his colleagues at the University Technical Services for their cooperation in the preparation of models, and

Mr. T. Dyer for the help in drafting.

This study at Memorial University would not have been possible without the leave of absence granted by the Public Works Department, Government of Bihar, India, which is gratefully acknowledged.

The cooperation of Mrs. Margaret Rose in typing this thesis within a short period of time is acknowledged with thanks.

TABLE OF CONTENTS

LIST OF TABLES

LIST OF FIGURES

NOTATIONS

The symbols listed below and used in this thesis generally conform to those suggested by the American Society of Civil Engineers (Nomenclature for soil mechanics, Journal of the Soil Mechanics and Foundations Division, June 1962) and the Canadian Geotechnical Journal. They are also defined when they first appear in the text. SI Units are used throughout.

A - vertical surface area of the object in contact with soil

A_b - projected area of the base of embedded object

A_{max} - horizontal projection of maximum contact area

A_s - side surface area of failure prism

A_x - base surface area of failure prism

B - breadth or least lateral dimension of the embedded object

B_s - soil buoyancy force

B_w - water buoyancy force

C_A - vertical component of adhesion along soil-object interface

C_{AB} - cohesive resistance along soil failure plane

C_{ia} - initial adhesion at $T = 0$

C_{ta} - vertical component of adhesion on the top curved surface of the object

c - unit soil cohesion

$\bar{c}$ - unit soil cohesion averaged over embedment depth

c_a - unit soil adhesion averaged over embedment depth along vertical object-soil interface

c_b - unit cohesion at base level of the embedded object

c_u - undrained shear strength of clay

c_{ur} - residual undrained shear strength of clay

D - depth, embedment depth

F - breakout force

F_a - applied force to breakout

F_{Ib} - immediate breakout force

F_n - net breakout force

F_r - soil resistance

F_u - a dimensionless parameter $(= \frac{P_u - \gamma g D}{c})$

g - acceleration due to gravity

L - object length

L.I. - liquidity index

P - additional load to pull out or breakout

P_s - base suction force

p_s - unit base suction

p_u - unit ultimate uplift resistance

q_d - average supporting pressure provided by soil to maintain embedded object in equilibrium

R - soil shearing resistance along failure plane, resultant force acting on an object settling on sea floor

R_v - vertical component of R

S - representative undrained shear strength of soil

T - period of sedimentation

t - time, time allowed for breakout (in seconds)

W - weight of a sinking soil particle, counter balancing load

$\bar{W}$ - weight of the embedded object and the connecting cable in air

W_s - weight of soil above embedded object involved in breakout

$\bar{W}_s$ - soil buoyancy

α - adhesion to cohesion ratio

β - a dimensionless parameter $(= \frac{p_s}{c_b})$

γ - mass density of soil

γ_t - average saturated unit weight of soil

δ - angle of skin friction

σ - bearing strength of soil

ϕ - angle of internal friction in soil

SYMBOLS

cm - centimeter

kN - kilonewton

kPa - kilopascal

m - meter

mm - millimeter

Pa - Pascal

μ, μm - micrometer $(= 10^{-4} m)$

CHAPTER I

INTRODUCTION

1.1 General

There is a growing world-wide interest in the exploration, production and utilization of offshore oil, natural gas and other minerals. As a part of these efforts, interest has been directed in the last decade towards marine geotechnology. A number of offshore and undersea structures feature some degree of mobility in order to permit inspection and repair. This, in turn, requires that the structure be recovered and replaced periodically, e.g., the case of laying and relocating marine pipelines, exploratory oil rigs such as the Jack up platforms, well-linings, well-head manifolds, placing and refloating bottom-sitting gravity structures, etc. Another problem associated with the recovery operations is that of the salvage of wrecked and fully or partially sunken vehicles and objects.

Following the loss of the U.S. Navy submarine *Thresher* in 1963 (Muga, 1968) and the subsequent loss of a nuclear weapon in 1966 after a mid-air collision of a bomber and its refuelling tanker off the coast of Spain, increased interest has been shown in the study of the salvage and retrieval of objects embedded in ocean sediments.

Objects embedded in soils, either partially or fully, require forces greater than their own weight to dislodge them. This additional force requirement, termed the breakout problem, is of great importance in the planning and execution of many Naval undersea operations. Among these are the salvage of sunken vessels and ordnance, the retrieval of bottom-sitting devices or structures, and the use of embedded anchors. In each of these cases it would be desirable to be able to predict in advance the magnitude of the breakout force so that the equipment for the operation could be selected and used appropriately.

The problem of breakout is extensive and has a number of variables. However, it is possible to divide it into sub-problems which are less broad and, therefore, simpler to study. Individual studies can be made on the effects of object embedment depth, soil type, nature of object surface, shape, and the type of breakout operation.

The type of breakout operation can be classified into two categories - immediate and aided breakout. Immediate breakout involves only direct lifting pull on the embedded object being dislodged from the soil medium; aided breakout includes the performance of other activities, e.g., water jetting, excavation beneath the object, and rolling the object prior to force application for pull out.

Adhesion studies have an important application to the cold oceans in the studies of ice-soil interaction. To date,

not much research appears to have been done on this aspect.

1.2 Scope of the Present Investigation

As in any other engineering research, the breakout problem could be investigated theoretically, experimentally in a laboratory, or by full scale testing. The study reported here is confined to laboratory work.

The objectives of the laboratory experiments are to determine:

1. The interaction between an object and a weak soil at its interface during the pull out of partially embedded plates. This will give the adhesive resistance between the sides of the object and soil.
2. The interaction at the object-soil basal interface in the case of partially embedded prismatic models.
3. The breakout phenomenon of fully embedded objects of different shapes, and
4. Adhesion between ice sheets and soil. These ice sheet studies were done in a cold room at a temperature of $-3^{\circ}C$.

Relatively greater emphasis was placed on the experiments with plate models in which plates of different materials and roughness were tested. Results from these series of tests were used in the analysis of the results under categories 2 and 3. A more detailed description of the tests is given in Chapter III.

Artificially sedimented potter's clay (modeling clay) was used in this work, to simulate the weak, underconsolidated surficial ocean sediments. Details of the test program, the various types of tests and the analysis of the results are given in Chapters III to V.

CHAPTER II

REVIEW OF LITERATURE

There are many historic records of maritime salvage operations describing the retrieval of sunken ships from mud bottom under very unfavorable circumstances. The breakout problem discussed herein is not intended to be an all inclusive treatment of ship salvage. Only those cases where the breakout force was referenced in the published literature have been selected for review. The mechanics of breakout and the experimental work reported in the literature are reviewed.

A review is also given of the properties of surficial ocean sediments and their uniqueness as a separate class of soil.

2.1 Examples of Maritime Salvage Operations

The earliest known published report on salvage operations (Muga, 1968) is that of *Södra Sverige*, a cargo steamship of 6000 kN displacement, which sank in the Baltic Sea in 1895 in a water depth of 60 m. During the course of a year, it settled about 3 m into the clay bottom. Calculations indicated that a force of 9600 kN was required to break the ship loose from the bottom.

S-51, a U.S. Navy submarine sank in 1925, approximately 30 km east of Rhode Island in the Atlantic Ocean.

The water depth at this site was 43 m where the submarine came to rest on a clay bottom. The breakout force was estimated at 8000 kN, in addition to the submerged weight of the submarine which was estimated at 10,000 kN. In order to dislodge the submarine, water jetting in between the hull and the sediment was done to break the suction at the soil-hull interface.

S-4, a boat which sank in 1927 in 30 m waters off Provincetown, Massachusetts (U.S.A.) was buried in a layered soil to a depth of 2 to 2.5 m. The texture of the soil at the hull contact was sandy and permitted easy drainage of water. Due to the permeable character of the soil it was reported that the 'suction effect' on the submarine was practically nil.

The salvage of the *USS Squalus* is perhaps the most widely reported and well documented of all marine salvage operations. It sank in 1939 about 8 km south of the Isles of Shoales off Portsmouth Harbor in Rhode Island. Although no estimate of breakout force was given, it was reported that an unknown amount of mud suction, tending to hold down the bow, was one of the main factors contributing to the unsuccessful lift.

Yet another reported study of the predominance of mud suction is that of the deployment and recovery of the 60 m long floating blocks of reinforced concrete (PHOENIXES). These were to be sunk in a line off the Normandy beach to

provide a breakwater during the European invasion in 1944. Approximately 100 of these PHOENIXES were purposely sunk in staging areas off the south coast of England prior to invasion. The first attempt to refloat a PHOENIX by pumping out water failed. It was determined that mud suction was holding the PHOENIX down. However, quantitative data of this operation is not available.

In summary, the problem of freeing naval vessels from the ocean bottom has been recoghized for a long time. But the analysis of this problem based on the basic principles of soil mechanics is only of recent origin.

2.2 Studies on Breakout Resistance

After the loss of the U.S. Navy submarine *Thresher* in 1963 (Muga, 1968), an intensive research program was sponsored by the U.S. Navy and the Naval Civil Engineering Laboratory at Port Hueneme, California, for the study of pull out or breakout force to lift a sunken object from the sea bottom. This includes analytical and laboratory model studies, as well as sea trials. These studies ultimately aim at determining the breakout force necessary to pull out an object, either fully or partially embedded. Figure 1 shows the mechanics of breakout. The breakout force F consists of the following five components for objects fully embedded:

(1) the effective weight of the object in soil ($\bar{W}$-$\bar{W}_s$), where $\bar{W}$ is the weight of object and the connecting cable in air

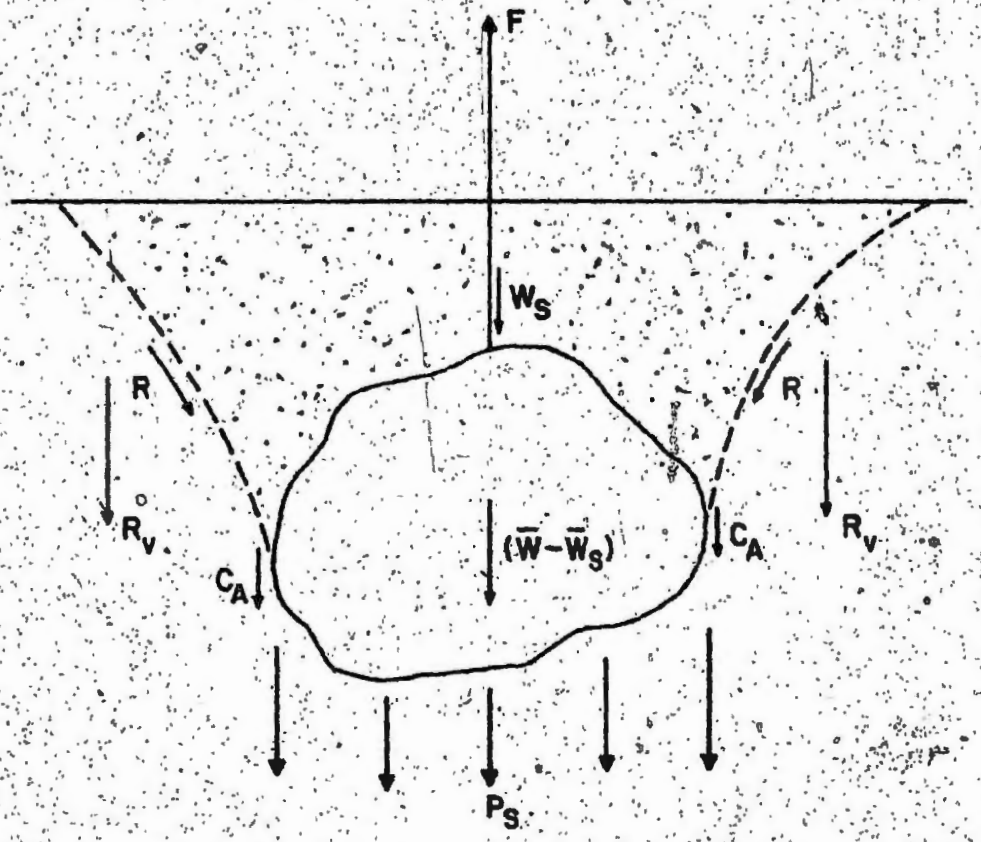

Fig. 1 MECHANICS OF BREAKOUT (Vesic, 1971)

and $\bar{W}_s$ is the soil buoyancy; (2) the effective weight of the soil mass, W_s; (3) the vertical component, R_v, of the shearing resistance R of the overburden soil along the slip surfaces; (4) the vertical component, C_A, of forces of adhesion at soil-object interface; and (5) the soil suction, P_s, at the base. The soil suction is due to the difference in pore-water pressures above and below the embedded object induced at the onset of the vertical upward movement of the system.

Experiments with objects embedded to various depths have been reported in the literature. Muga (1966) has reported experiments with 112 cm dia. spheres and 122 cm x 183 cm cylinders. There was considerable scatter in the results. Muga (1968) developed an analytical method to determine the force F necessary to break out an embedded object from the ocean floor based on three parameters - the average supporting pressure q_d provided by the soil to maintain the equilibrium, time t allowed for breakout, and the horizontal projection of maximum contact area A_{max}. The following empirical formula for the breakout force, based on field tests in San Francisco Bay, was arrived at.

$$F = 0.20\, A_{max} \cdot q_d \cdot e^{-0.00540(t-260)} \qquad [1]$$

Liu (1969) developed a general equation for breakout force of embedded objects in fine clay. Figure 2 shows the

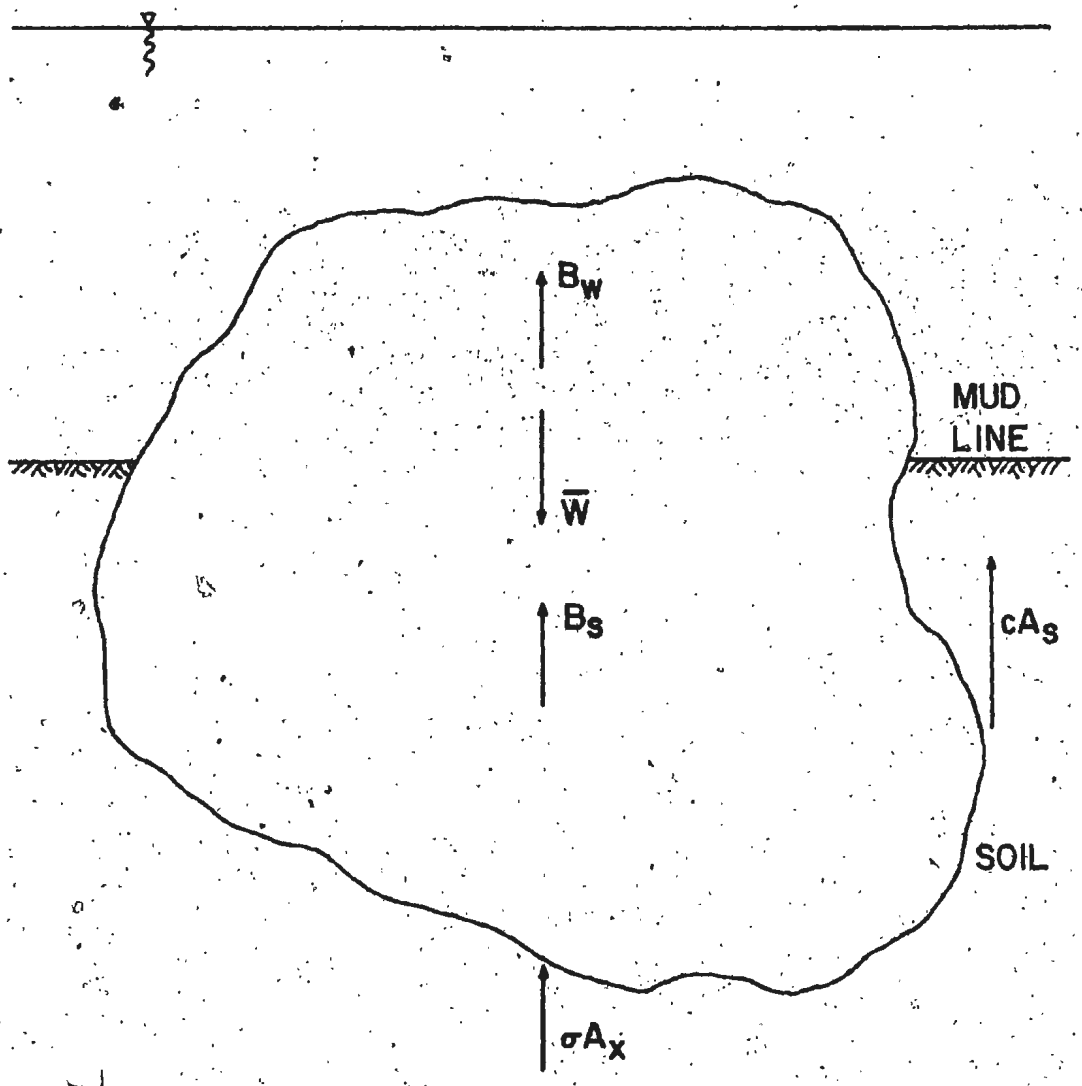

Fig. 2 CONCEPTUAL DIAGRAM SHOWING THE FORCES ON A SINKING OBJECT

(Liu, 1969)

forces acting on an object settling on the sea floor. The resultant force R was expressed as

$$R = \bar{W} - B_w - B_s - cA_s - \sigma A_x \quad [2]$$

where

$\bar{W}$ = dry weight of the object

B_w = water buoyancy force

B_s = soil buoyancy force

c = undrained shear strength of soil

σ = bearing strength of soil

A_s = side surface area of failure prism, and

A_x = base surface area of failure prism.

When an external upward pull F_a is applied, the resultant upward force on the embedded object was given by the expression

$$R_1 = F_a - (\bar{W}-B_w-B_s) - cA_s - \sigma_t A_x, \text{ where } \sigma_t \text{ is the soil tension strength}$$

or $$R_1 = F_n - F_r \quad [3]$$

where

$F_n = F_a - (\bar{W}-B_w-B_s)$, the net breakout force and

$F_r = cA_s + \sigma_t A_x$, the soil resistance.

Equation [3] implies that for $R_1 = 0$, i.e., when the net breakout force is equal to the soil resistance, a condition of incipient breakout exists. Hence,

$$F_n = F_r \quad [4]$$

While calculating the soil resistance, Liu (1969) assumed that the object-soil adhesion is stronger than the soil cohesion. For a prism, the failure was assumed to occur in the soil rather than along the wall of the object. According to Muga (1966, 1968), Liu (1969) and Vesic (1971) when an embedded object is being pulled out, the overburden soil is gradually compressed, whereas the soil immediately below the object is relieved of the bearing stress. There will be a decrease in pore-water pressure below the object so long as the permeability of soil does not respond immediately to the stress change. Figure 3 explains this phenomenon. This difference results in suction at the base of the object, termed as 'base suction'. Vesic (1971) proposed an analysis based on the cavity formation below the object. Soil suction effect is significant only in those soils whose natural water content is less than the liquid limit. This hypothesis is not applicable for soils which flow when the object is pulled out. Soil flow can occur if the liquidity index is high and the corresponding in-situ density of soil is too low.

Lee (1972) suggested an approximation for immediate breakout force in the form of bearing capacity equation as:

$$\frac{F_{Ib}}{A} = 5S \left(1.0 + 0.2 \frac{D}{B}\right)\left(1.0 + 0.2 \frac{B}{L}\right) \qquad [5]$$

where

F_{Ib} = immediate breakout force

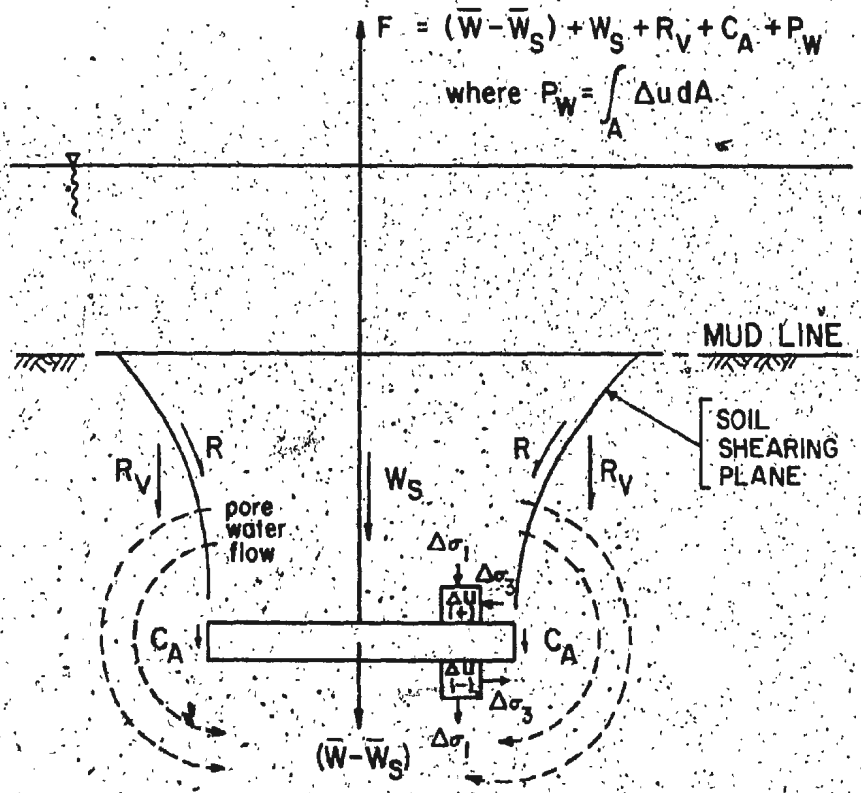

Fig. 3 DEVELOPMENT OF BASE SUCTION DUE TO DIFFERENTIAL PORE-WATER PRESSURE

(Vesic, 1971)

S = representative undrained shear strength of soil

L = object length

B = smallest lateral object dimension, and

D = embedment depth.

This equation showed good agreement with field tests.

Byrne and Finn (1978) reported results of small scale laboratory tests on breakout of objects submerged in marine clay (undisturbed shear strength = 50 kPa). They predicted the breakout force based on Hansen's (1961) bearing capacity formula which includes corrections for depth, shape and inclination. The ratio of base suction per unit area to the cohesion was experimentally obtained as 6.9, which is close to the value of 7.3 obtained from Hansen's bearing capacity formula.

Preliminary results of the adhesive resistance on plate models as a function of their surface roughnesses and shear strength were reported by Chari, et al. (1978). The ratio of base suction and cohesion based on pull out tests on prismatic objects partially embedded to different depths in clay of very low shear strength (c-62 Pa) was also reported and compared with those obtained using Lee's (1972) and Hansen's (1961) equations.

A dimensional analysis for soil uplift resistance, p_u, for perfectly smooth anchor plate and small diameter anchor shaft was made by Davie and Sutherland (1978). F_u, a dimensionless parameter, was introduced in the equation

for p_u as follows:

$$F_u = \frac{p_u - \gamma_g D}{c} \qquad [6]$$

where

D = depth of placement of anchor

c = cohesive strength of soil

γ_g = unit weight of soil, and

p_u = unit ultimate uplift resistance.

2.3 Marine Sediments

Ocean surface sediments have characteristics that are generally different from those found on land. Due to their depositional history, marine sediments remain under-consolidated as long as sediment deposition continues (Terzaghi, 1956). This type of soil is generally called mud in geological parlance and is characterized by high water content and low density and shear strength. Such soil could be present sometimes up to tens of meters depth. The primary source of sediment deposition in the oceans is transportation by rivers. It is estimated (Judson, 1968) that as much as 9.3×10^9 metric tons of sediments are carried annually by rivers into the oceans from continents. The depositional environment is an important factor contributing to the type of sediments in any particular location.

Terzaghi (1956) proposed a concept on the mechanics of sediment deposition. When a sinking soil particle with

weight W arrives at the surface of the sediment deposit (Figure 4) it tends to roll or slide into the most stable position. The tendency to slide is resisted by the adhesion between soil particles at the first point of contact. The resisting couple M_2 due to adhesion is independent of the grain size. The overturning couple $M_1 = W.r$ decreases as the fourth power of the grain size. This accounts for the varying void ratios with grain size. Any vibration causes a rearrangement of the particles. This type of soil structure was termed by Terzaghi as 'metastable'. It was found that particles with grain size between 20 and 6 microns corresponding to the conventional silt size are most sensitive to vibration. At the instant of collapse of the metastable structure, the weight of the solid particles is temporarily transferred from the point of soil contact to the water. Consequently the hydrostatic pressure at any depth increases resulting in liquefaction and flow of the soil. However, it is temporary. The flow of sediment is followed by expulsion of excess pore water and gradual increase in consolidation.

2.3.1 Mechanics of Underconsolidation

The classical description of underconsolidation in marine sediments is associated with the phenomenon of rapid sedimentation and the delay in pore-pressure dissipation under this increased total stress. Theoretical models of this mechanism have been postulated by Olsson (1949, 1958),

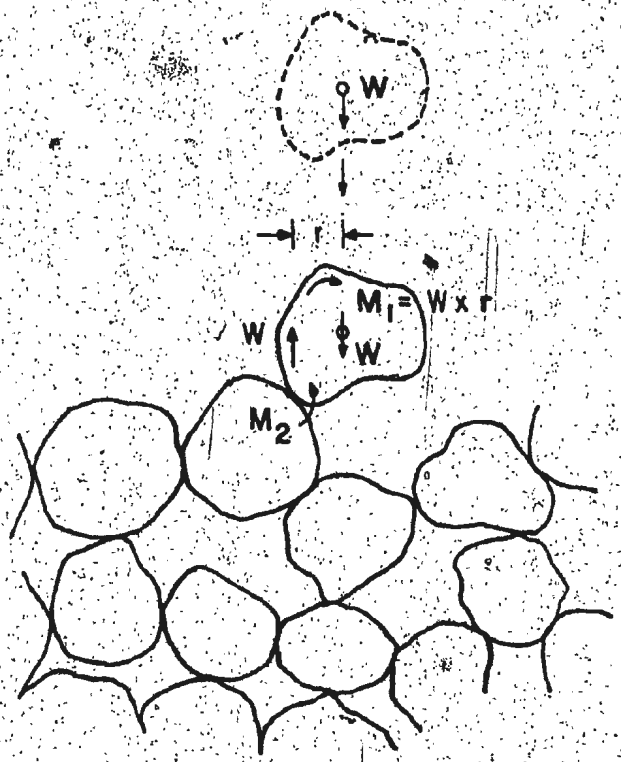

Fig. 4 CONCEPT OF METASTABLE STRUCTURE

(Terzaghi, 1956)

Terzaghi (1956), and Gibson (1958); there is also field documentation from areas of high accretion rates (Fisk and McClelland, 1959; McClelland, 1967). The key characteristic of underconsolidated soils, important from the standpoint of stability is the amount and distribution of excess pore-water pressure.

In addition to the rapid accretion rate, there are at least three other possible causes of underconsolidation (Sangrey, 1977) in marine sediment, as illustrated in Figure 5. These are (1) presence of gas in marine sediments, (2) leakage from an artesian water or gas pressure source, and (3) repeated loading. Each of these mechanisms is unique and the magnitudes and distribution of excess pore pressure are different. In all cases, however, the excess pore pressure presents similar problems of lower shear strength and increased potential for instability of the marine sediments.

2.3.2 Types of Marine Sediments

The surficial ocean sediments are not of the same type everywhere throughout the ocean basins. It depends on the depositional history in the ocean basins and the diagenesis since their formation. The sediment size depends on the depositional environment and the proximity of the shore. Generally deep ocean sediments are fine grained. Keller (1967) has classified marine sediments under five broad categories as:

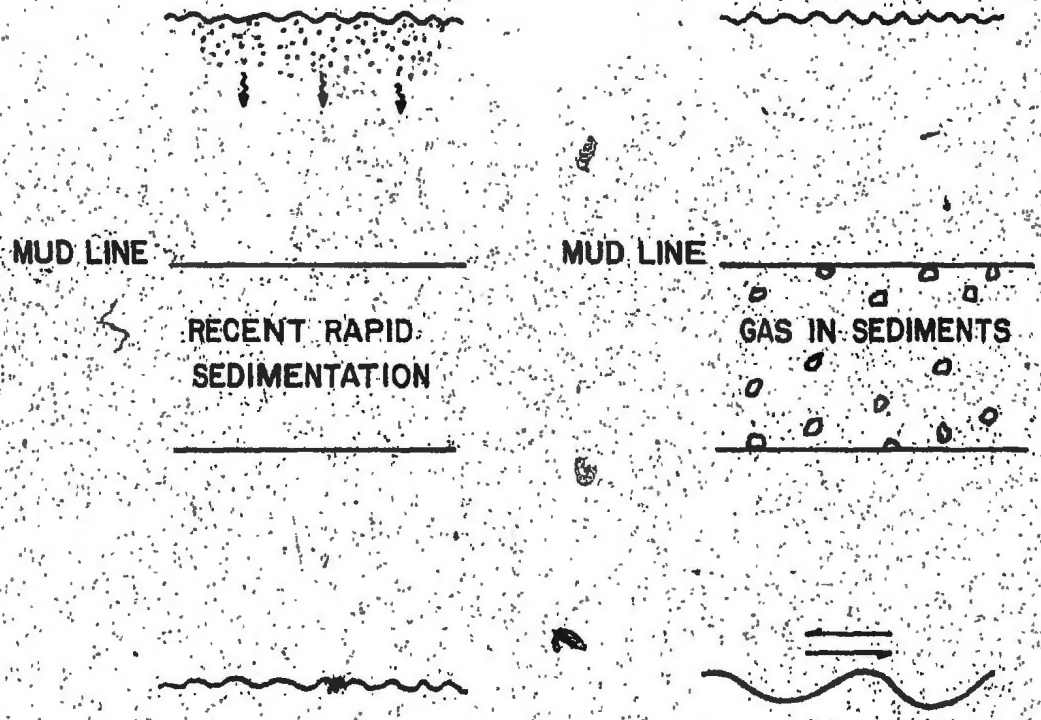

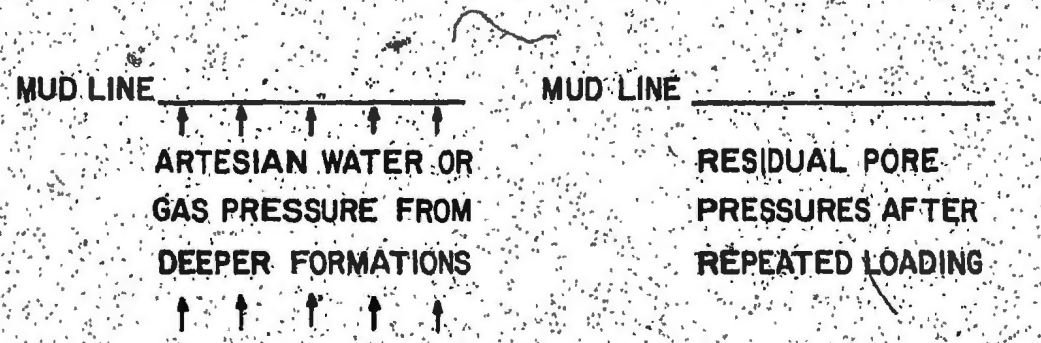

Fig. 5 MECHANISMS OF UNDERCONSOLIDATION

(Sangrey, 1977)

(i) Fluvial-marine (sand-silt); (ii) Fluvial-marine (silty-clay); (iii) 'red clay', a term applied to inorganic pelagic clays; (iv) calcareous ooze; (v) calcareous sand and silt. Each type has a different range of properties.

2.4 Engineering Properties of Marine Soil

Till recently, the study of marine sediments has been a subject of interest to marine geologists with an intent to study the depositional history and geology. With the increased pace of offshore exploration for oil and natural gas, the huge structures that are to be placed on the ocean floor have to be designed to satisfy all considerations. At this time, information on the engineering properties of sea floor sediments is scarce. Synoptic data on the various sediment properties in the North Atlantic and the Pacific, as well as other places, are available in various publications (Davie, et al., 1978; Helwick and Bryant, 1977; Keller, 1967; Noorany and Gizienski, 1970; Silva, et al., 1976). Table I is a summary compiled from these publications and gives the range of variability of the different properties.

2.5 Adhesive Resistance of Clays

Mud suction or base suction is one of the forces resisting breakout of objects and has been discussed in para. 2.2. In addition to this base suction, there is an adhesive force at the interface of the object sides and soil. Published

TABLE I

ENGINEERING PROPERTIES OF OCEAN SEDIMENTS

Location	Clay particles less than 2μ %	Clay Minerals: Chlorite %	Montmorillonite %	Illite %	Kaolinite %	Wet unit weight (kN/m³)	W.C. %	P.L. %	L.L. %	Average Shear Strength (kPa)
North Atlantic	–	10 (27)	16 (27)	55 (27)	20 (27)	15–17 (17)	50–100 (17)	–	–	3–6 (17)
North Atlantic* (Hudson Cruise)	40–50	–	–	–	–	12–15	80–100	40–50	70–100	8–12
North Pacific	–	18 (27)	35 (27)	40 (27)	8 (27)	15–16	100–200 (17)	–	–	<3 (17)
Pacific Ocean (5)	62**	–	–	–	–	13.8	80–119	–	–	<10
Indian Ocean & Arabian Sea										
East Bay Area, Mississippi Delta (15)	–	–	–	–	–	–	23–119	20–30	24–100	<10
Bermuda Rise (32) (Hummock region)	51	6–12	14–23	52–66	5–8	–	90–150	37–51	86–161	4

Numerals in parentheses indicate reference numbers.

* Results of tests on core samples collected during May 1978 cruise on C.S.S. Hudson (to be published)

** Less than 4μ

literature on adhesive resistance of underconsolidated ocean bottom sediments is limited.

The property of adhesion, particularly for deep foundations in clay, is well documented in soil mechanics literature. For *piles* in soft clay, a major part of the load transfer is by shear resistance at the soil-pile vertical interface. This resistance, which is generally termed the adhesion, is a basic soil property and is generally expressed as a fraction of the soil cohesion. In c-ϕ soils, shear resistance at the soil-pile interface is also influenced by skin friction. The angle of skin friction, usually denoted by δ, is expressed as a function of the basic angle of shear resistance for the soil.

Considerable work on the adhesion and skin friction at the interface between construction materials and terrestrial soils has been done and reported. Meyerhof and Murdock (1953) reported results of shear box tests conducted to determine adhesion at the interface of stone and clay. The shear strength of clay used in the experiments was in the range of 96 to 287 kPa. With a normal pressure in the order of 107 kPa, the value of the adhesion to cohesion ratio (α) was 0.8 in the case of dry stone and 0.4 for the same stone in a wet condition. It was also reported that for large normal pressures, adhesion approached the soil shear strength. Potyondy (1961) determined from direct shear tests the value of α to be 0.84 for rough steel and 0.51 for smooth steel.

The cohesion of the soil used in the test was 56 kPa with a ϕ of 16.5°. Witney (1968) reported a value of α for glass plate and clay (c = 13 kPa) as 0.11. Littleton (1976) determined the values of α for kaolinite and illite with smooth steel. In these experiments, the quantitative value of the specimen roughness was determined using the Taylor-Hobson No. 3 Talysurf machine and expressed as center line average of 0.18 μm with a cut-off length of 0.84 mm. The value of α was found to be 0.91 for kaolinite (c = 9 kPa) and 0.84 for illite (c = 25 kPa).

Wang, et al. (1977) reported the values of α between clay and acrylic to be 0.75 for c = 552 Pa, and 0.67 for c = 1.0 kPa.

Erchul and Smith (1969) investigated the resistance to penetration of objects, such as coring tools, into ocean sediments. Coated and uncoated stainless steel plates were embedded in a sediment having a cohesion of 7.2 kPa. The maximum sediment adhesion for uncoated stainless steel plates was reported to be in the range of 1.2 to 1.7 kPa which gives a range of 0.17 to 0.24 for α values. α for coated plates was found in the order of 0.16 to 0.20.

It is seen from the literature reviewed that the values of the adhesion-cohesion ratio vary over a wide range. It is also observed that quantitative values for object surface roughness have not been reported in most publications. Research on the adhesion of weak underconsolidated sediments

is still in its infant stage and so is that on ice-soil interaction.

These aspects are examined in some detail in this thesis.

CHAPTER III

EXPERIMENTAL FACILITY AND TEST PROGRAM

Experiments were designed to determine the soil adhesion along the vertical soil-object interface for partially embedded plate models, base suction at the object bottom for partially embedded prismatic models and the total breakout load in the case of fully embedded models of different shapes.

3.1 Experimental Facility

The experimental facility consists of a glass sided circular container of about 30 cm. internal diameter and 28 cm. height. Soil slurry was prepared in the container with 14.8 kg. of dry soil in 13.24 liters of fresh water. The test model was suspended vertically from a load cell which, in turn, was supported by a counter weight placed on the other side of the pulley. Details of the arrangement are shown in Figures 6 and 7. A strain gage indicator was used in conjunction with the load cell. Direct record of the load variation was also plotted on an X-Y plotter. The vertical movement of embedded object was monitored by a pointer sliding on a potentiometer wire and plotted directly on the Y-axis of the X-Y plotter.

Fig. 6 PHOTOGRAPH SHOWING LABORATORY FACILITY

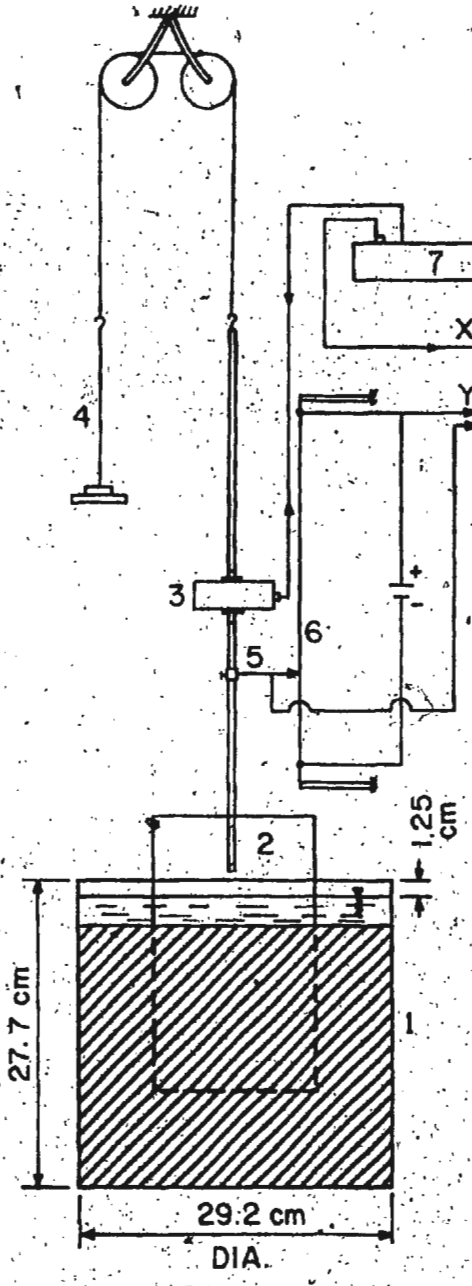

Legend

1. Glass Container With Soil
2. Plate Model
3. Flat Load Cell
4. Hanger With Load
5. Slider
6. Potentiometer Wire
7. Strain Gage Indicator
8. X-Y Plotter

Fig. 7 SCHEMATIC DIAGRAM SHOWING EXPERIMENTAL ARRANGEMENT

3.2 Soil Properties

The soil used in the present investigation was commercially available potter's clay. Figure 8 shows the grain size distribution for the soil. The mineralogical composition of the soil was determined by X-ray diffraction method (Mitchell, 1976). The most predominant minerals found were illite, chlorite and kaolinite. Traces of quartz and haematite were also present. Only qualitative mineralogy was determined due to equipment limitations.

Figure 9a shows an electron photomicrograph of the soil sample as seen through a scanning electron microscope. In order to get the stereo effect on the photomicrograph another electron photomicrograph of the same sample was taken (Figure 9b) at an inclination of 8° to the horizontal. The flaky nature of the soil particles was verified while viewing the two photomicrographs through a stereo microscope. The particle surface itself is not exactly plane, but oval at the top. A summary of the properties of the soil used is given in Table II.

3.3 Preparation of Soil Slurry

The soil slurry was prepared by manual mixing, making sure that all lumps were thoroughly kneaded and well mixed. All the experiments were conducted at room temperature (20°C) except those with ice sheets, which were carried out in a cold room at a temperature of -3°C. The soil slurry used

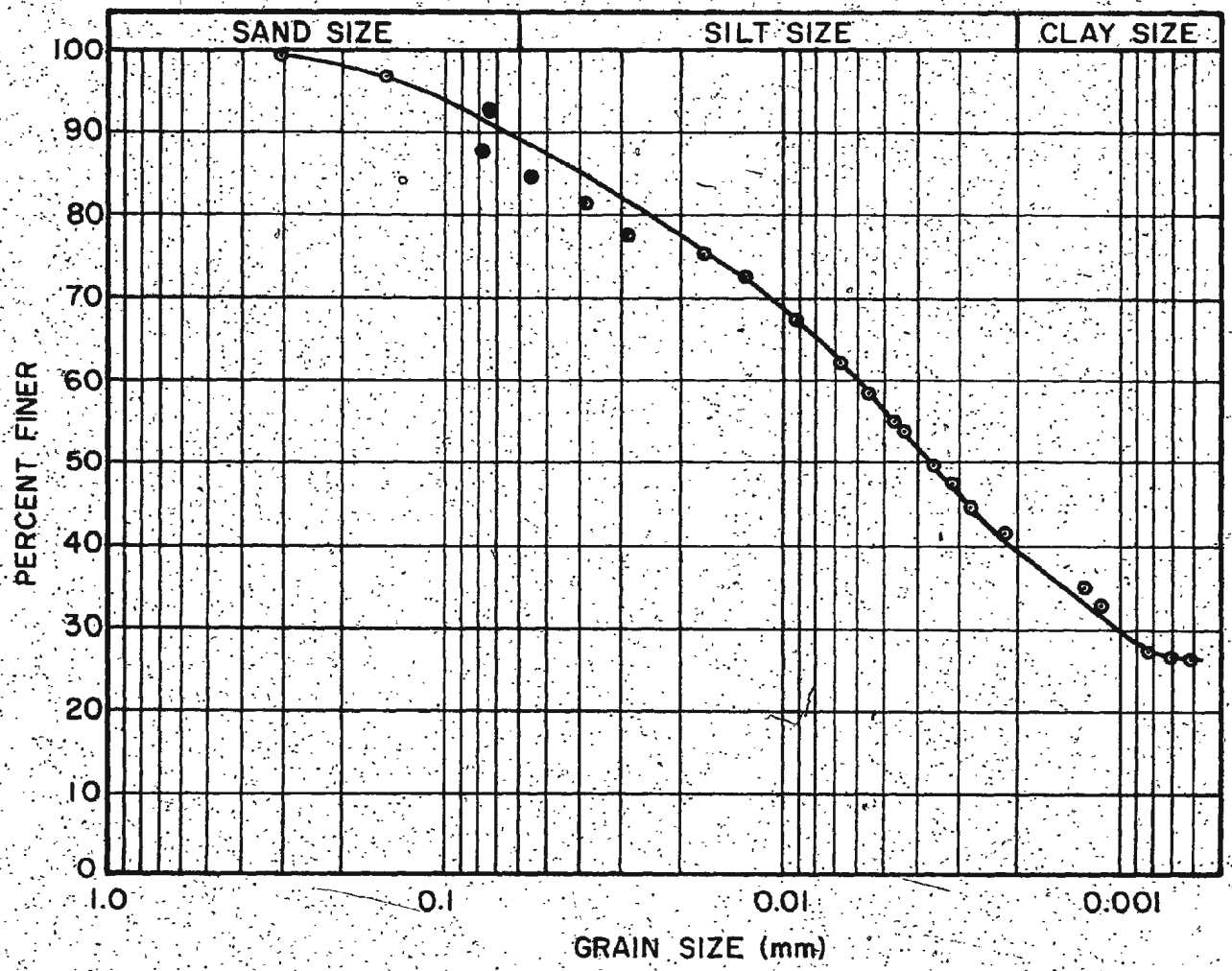

Fig. 8 GRAIN SIZE DISTRIBUTION OF SOIL

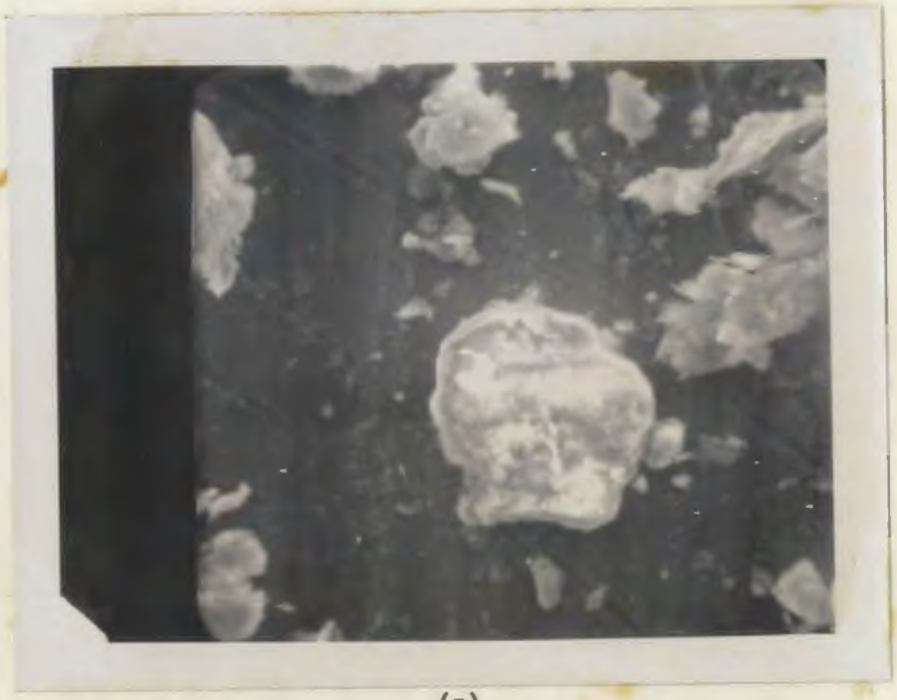

(a)

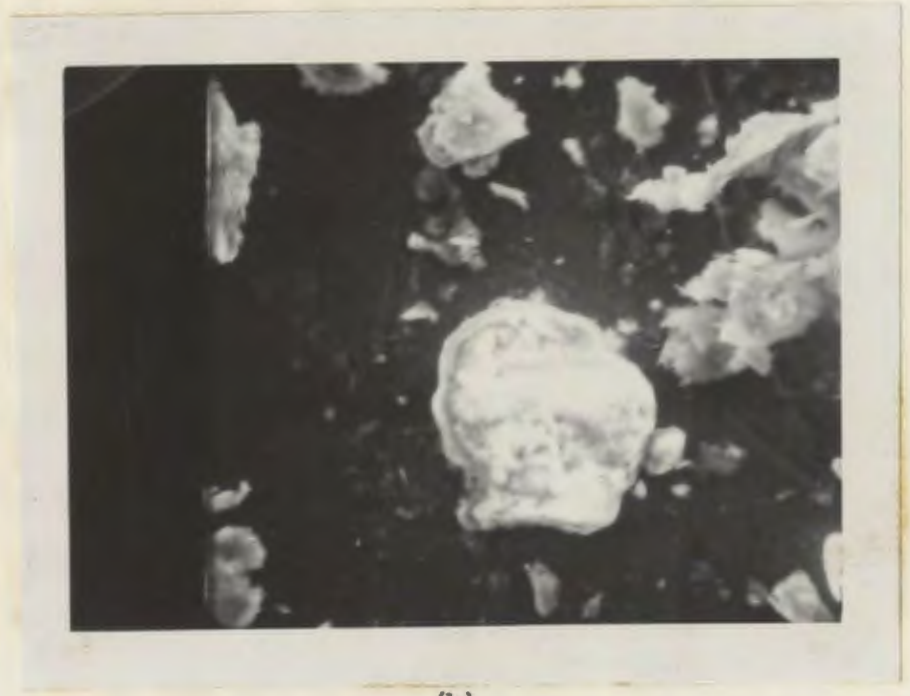

(b)

Fig. 9 STEREOSCOPIC PAIR OF AN INTACT SOIL SPECIMEN SHOWING CLAY MINERALS (MAGNIFICATION = 2000)

TABLE II

PROPERTIES OF SOIL USED IN THE EXPERIMENTS

Visual classification	Brown silty clay
Liquid limit (%)	30
Plastic limit (%)	16
Plasticity index	14
Classification symbol (Unified classification system)	CL
Clay size (less than 2μ)	40
Silt size	51
Sand size (greater than 60μ)	9
*Specific gravity of solids	2.73
Clay minerals	Predominantly illite, chlorite and kaolinite. Traces of quartz and haematite are found.
Activity = $\frac{P.I.}{C-n}$ (Mitchell, 1976)	0.47

where
P.I. = Plasticity index
C = Clay content (%) less than 2μ, and
n = 10, for artificially prepared clay

* The term 'Specific gravity' is replaced by 'Relative density' in contemporary Geotechnical publications.

for ice sheets contained 25 percent antifreeze (ethylene glycol) by volume and the slurry concentration was kept the same by removing an equal amount of water.

Since the same soil was used in all the experiments, great care was taken to ensure that no material was lost during the change over of the models. The soil grain size distribution was checked once during the progress of the experimental program and also at the end to verify that the clay size fraction was constant.

From the known weight of dry soil used and the relative density of the grains (specific gravity), the bulk density (unit weight) of the soil sample was determined by measuring the height of the soil in the glass container. Periodic checks were also done by immersing a thin walled aluminum ring (7.31 cm. diameter, and 7.27 cm. height) and taking out a sample after sliding thin glass plates at the ends of the ring.

Since only one type of soil was used, the period of sedimentation was an important variable. By varying the sedimentation period, different values were obtained for the soil unit weight, cohesion and liquidity index.

3.4 Types of Models

Ice sheet, glass plate, plexiglas, brass, painted mild steel, stainless steel and rusted mild steel of two different surface roughnesses were selected for plate models

to cover a wide range of surface roughness as well as to represent a variety of materials.

A quantitative evaluation of the surface roughness of these materials (except ice sheet) was made by using Taylor-Hobson No. 4 Talysurf and a rectilinear recorder. The equipment is shown in Figure 10. The roughness is expressed (CSA B95: 1962) in terms of center line average (CLA) in microns over a cut-off length of 0.254 mm. The measured roughness values are presented in Table III.

Prismatic models were all made of plexiglas. In prismatic models, the suction at the base-soil interface is a force developed during pull out in addition to the adhesion on the sides. Three configurations for the base were chosen to observe the effect of base shape on the pull out force. The configurations were (a) flat base, (b) projecting tapered base, and (c) dished base.

For tests with fully embedded objects, some common shapes such as a cube, a right circular cylinder, a sphere and a hemisphere were used.

The ice sheet used in the experiment was about 1.25 cm. thick and was prepared from fresh water in a cold room at a temperature of $-3^{\circ}C$. A 3 mm. thick flat wooden piece was cast with the ice sheet centrally at the top end to facilitate connection with the load cell.

Fig. 10 PHOTOGRAPH SHOWING TAYLOR-HOBSON NO. 4 TALYSURF AND RECTILINEAR RECORDER

TABLE III

SURFACE ROUGHNESS OF MATERIALS OF PLATE MODELS

Material (25 cm. x 15 cm.)	Surface roughness expressed as center line average over a cut-off length of 0.254 mm (μm)
Glass plate (GP)	0.00762
Plexiglas (PG)	0.03048
Brass (BR)	0.04445
*Painted mild steel (MSP)	0.1778
Stainless steel (SS)	0.1905
Mild steel rusted - II (MSR II)	2.1950
Mild steel rusted - I (MSR I)	3.9370

* with commercial red marine enamel

3.5 Test Program

The laboratory investigation was carried out in four phases:

3.5.1 Plate model tests

Pull out tests were carried out in which the amount of pull necessary at the onset of pull out was recorded. A total of 50 pull out tests were conducted in this category. Tests on plexiglas plates were extensive and conducted at the end of sedimentation periods of 2, 4, 6, 8, 10, 12, 14, 16, 20, 24, 48 and 72 hours. Based on a preliminary analysis of these results, it was determined that sedimentation periods of 2, 10, 16, 24, 48 and 72 hours were reliable representative intervals. For glass plate, brass, painted mild steel, stainless steel, mild steel rusted I, mild steel rusted II and ice sheet tests were conducted at these periods. A summary of all the types of tests is shown in Appendix B.

3.5.2 Tests on partially embedded prismatic objects

Prismatic models of plexiglas (Figure 11) having (a) flat base; (b) pyramidal base with apex angles of 90° and 135°; and (c) flat base with all round skirt were partially embedded in the soil and the pull out resistance after a desired period of sedimentation was recorded. These tests were conducted with plexiglas models. A total of 31 experiments were conducted in this class and listed in Appendix B. As already discussed in Chapter III, there are

three components to the breakout problem. These are (i) the adhesion on the sides of the object, (ii) the base suction, and (iii) the effect of the surcharge soil. Experiments on plate models determine the soil adhesion on the sides. Partially embedded objects offer resistance due to base suction and adhesion on sides when pulled out. By interpreting the results of experiments in categories 1 and 2, the base suction and adhesion components can be expressed separately. Computation details are discussed in Appendix A.

3.5.3 Tests on fully embedded objects

Plexiglas models of different shapes (Figure 12), viz., (a) cube; (b) right circular cylinder with longitudinal axis vertical; (c) right circular cylinder with longitudinal axis in horizontal attitude; (d) sphere; and (e) hemisphere were fully embedded to different depths and the breakout load in each case was recorded. Ten experiments were conducted in this category. The presence of soil on top is an additional factor in these tests. Results from the previous two categories of experiments were used in interpreting the tests on fully embedded objects and in computing all the three components of the breakout resistance.

3.5.4 Tests on ice sheets

These were conducted in a cold room with ice sheets which were cast as described in para. 3.4. These experiments are similar to those with plate models and aimed

Fig. 11 PHOTOGRAPH SHOWING PRISMATIC PLEXIGLAS MODELS WITH (1) FLAT BASE, (2) PYRAMIDAL BASE WITH APEX ANGLE 90°, (3) PYRAMIDAL BASE WITH APEX ANGLE 135°, AND (4) FLAT BASE WITH ALL ROUND SKIRT, USED IN PARTIALLY EMBEDDED PULL OUT TESTS

Fig. 12 PHOTOGRAPH SHOWING PLEXIGLAS MODELS USED FOR FULLY EMBEDDED BREAKOUT TESTS: (1) CUBE, (2) RIGHT CIRCULAR CYLINDER (AXIS VERTICAL), (3) RIGHT CIRCULAR CYLINDER (LONGITUDINAL AXIS IN HORIZONTAL ATTITUDE), (4) SPHERE AND (5) HEMISPHERE

at determining the soil-ice adhesive force on the sides.

3.6 Test Procedure

The test procedure for all the categories of tests was as follows:

Soil slurry was first prepared by mixing the soil thoroughly with water. The model was then lowered to a predetermined depth and its weight in the slurry, weight of the load cell and the connecting rods were counter balanced with weights placed on the other side of the pulley. The weight of the model was thus balanced and there was no downward pressure on the soil at any time. The time of sedimentation was reckoned from the instant the slurry was made and the model lowered.

The soil was left undisturbed for the desired period of sedimentation. At the end of this period, the soil unit weight was computed as already explained. The cohesion of soil was then measured with a modified laboratory vane shear apparatus. Laboratory vanes having stainless steel blades of 5 cm. diameter by 2.5 cm. height were fabricated to facilitate measurement of very low shear strengths. The vane was rotated at 10°/minute. The cohesion was measured with top of vane flush with the surface and at depths of 5, 10, 15 and 20 cm. from the soil surface.

After measuring the soil strength, additional weights were placed in the pan in steps until the onset of

pull out. The pull out load was read on the strain gage indicator and simultaneously plotted on the X-Y plotter as a function of vertical movement of the model. The maximum pull out load was thus measured. Soon after completion of the test, the model was washed into the glass container so as not to lose any soil

It is to be pointed out here that the breakout loads determined in these experiments are the loads to pull out the object in a single effort. The total time for breakout varied from 30 secs to 2 minutes. Time effects by applying intermediate loads were not studied. A reference to Muga (1968) is made for details of time effects.

CHAPTER IV

RESULTS AND DISCUSSION

The different variables considered for this study are, the object roughness, object shape and the soil shear strength. The soil strength was varied by conducting tests after different periods of settlement of the slurry. Experimental results and their discussion are presented below:

4.1 Sediment Properties as a Function of the Time of Sedimentation

The sedimentation rate of the soil slurry was observed soon after the slurry was formed and settlement started. The relationship of the sedimentation with time is shown in Figure 13. The time-sedimentation curve becomes asymptotic after a period of about 72 hours. The maximum period of sedimentation in the test program was thus taken as 72 hours, a reference standard. The variation of the average unit weight (γ_t) of the soil with time is shown in Figure 14. The soil unit weight varies from 14.8 to 16.0 kN/m^3 in 72 hours, which is about 1.5 to 1.65 times the unit weight of water. The corresponding water content is in the order of 80 percent to 65 percent.

Liquidity index is a useful parameter for expressing and comparing the consistencies of different clays. It is

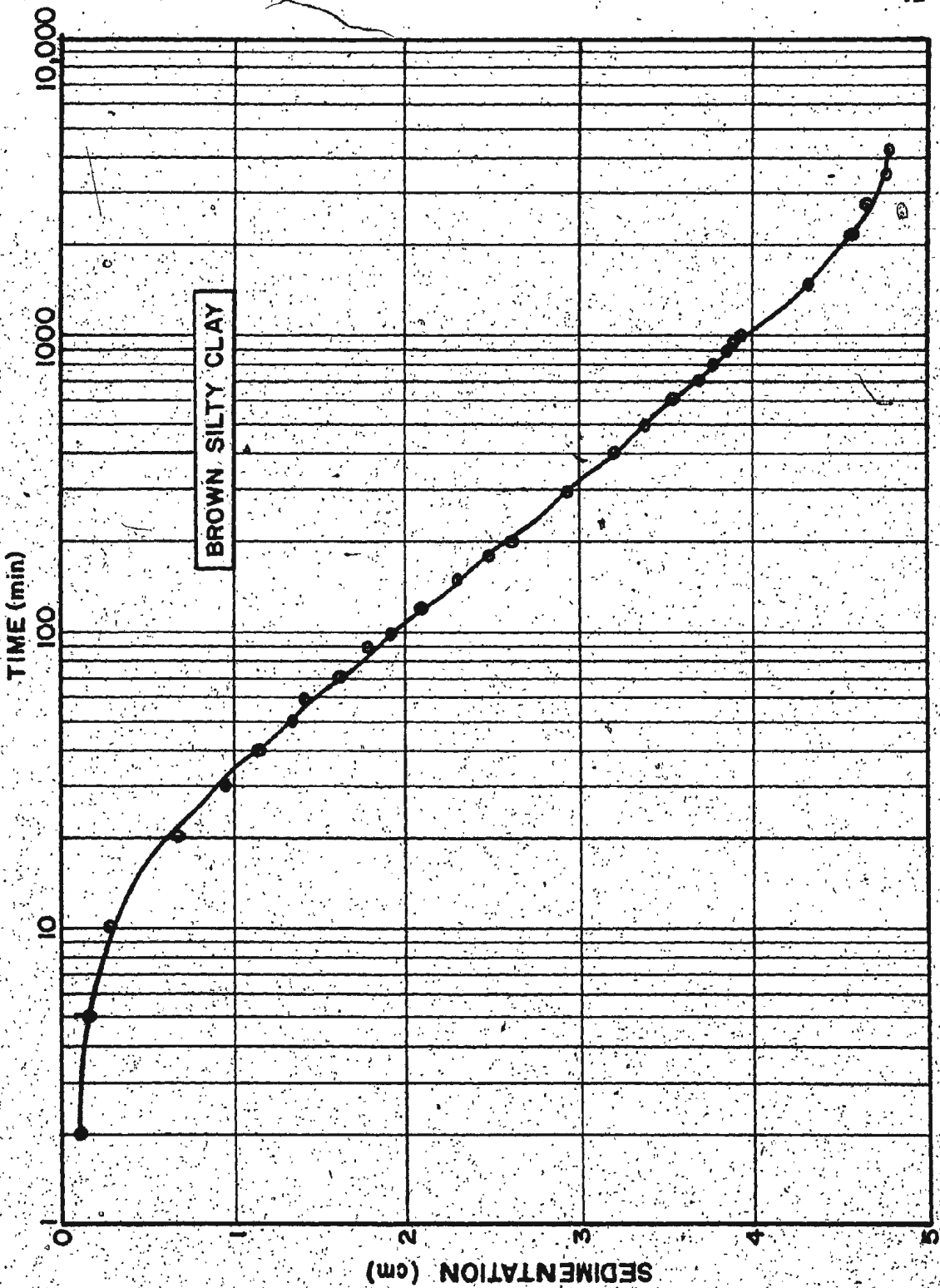

Fig. 13—TIME-SEDIMENTATION RELATIONSHIP

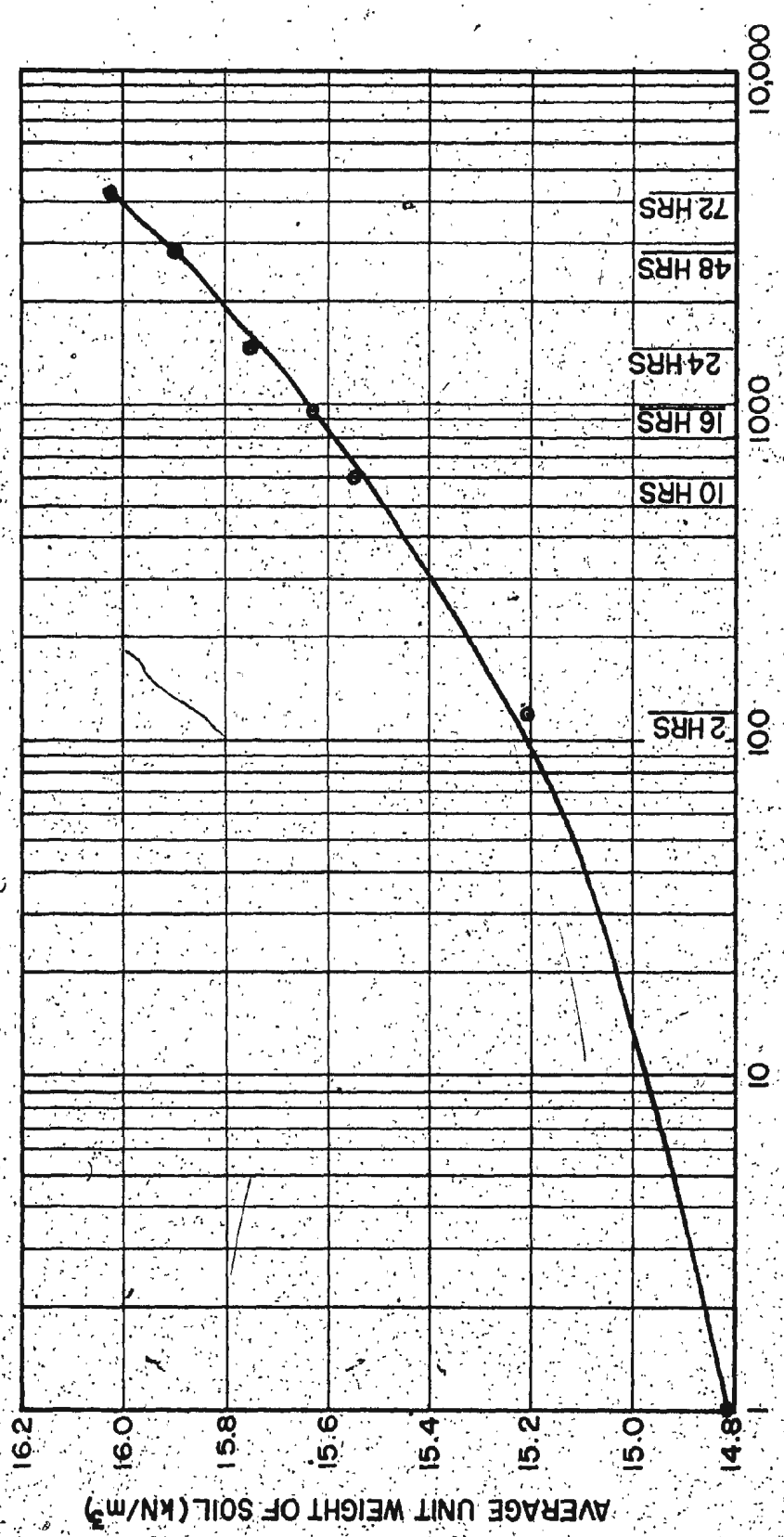

Fig. 14 RELATIONSHIP BETWEEN AVERAGE UNIT WEIGHT OF SOIL AND TIME OF SEDIMENTATION

given by L.I. = $\frac{\text{Water content - Plastic limit}}{\text{Plasticity index}}$.

The variation of liquidity index with the time of sedimentation is shown in Figure 15. The liquidity index varies from a high value of 4.5 in the slurry form to 3.4 after 72 hours. The high liquidity indices of soil used in these tests compare well with those obtainable in the highly underconsolidated ocean floor sediments (Silva, et al., 1976).

4.2 Plate model tests

In the analysis of all the plate model tests, the cohesion and adhesion were calculated as an averaged uniform value over the embedded depth of the plate. Results discussed here are for such averaged values.

4.2.1 Relationship between cohesion and time of sedimentation

The soil type used in this work is silty-clay, in a slurry and underconsolidated form. The soil cohesion is generally the primary component of the shear strength of such soils. The vane shear values obtained in the tests are used synonymous with the term cohesion, in the present discussion. The relationship between soil cohesion and the time of sedimentation is presented in Figure 16. The increase in cohesion is very slow in the initial period of sedimentation and is rapid subsequently. The slower rate of sedimentation during the initial period and also the slower development of the electro-chemical forces (Vanderwaal's forces) between flaky grains of the soil (Grim, 1968; Mitchell, 1976; Trollope, 1960) account for the slower increase of cohesion during

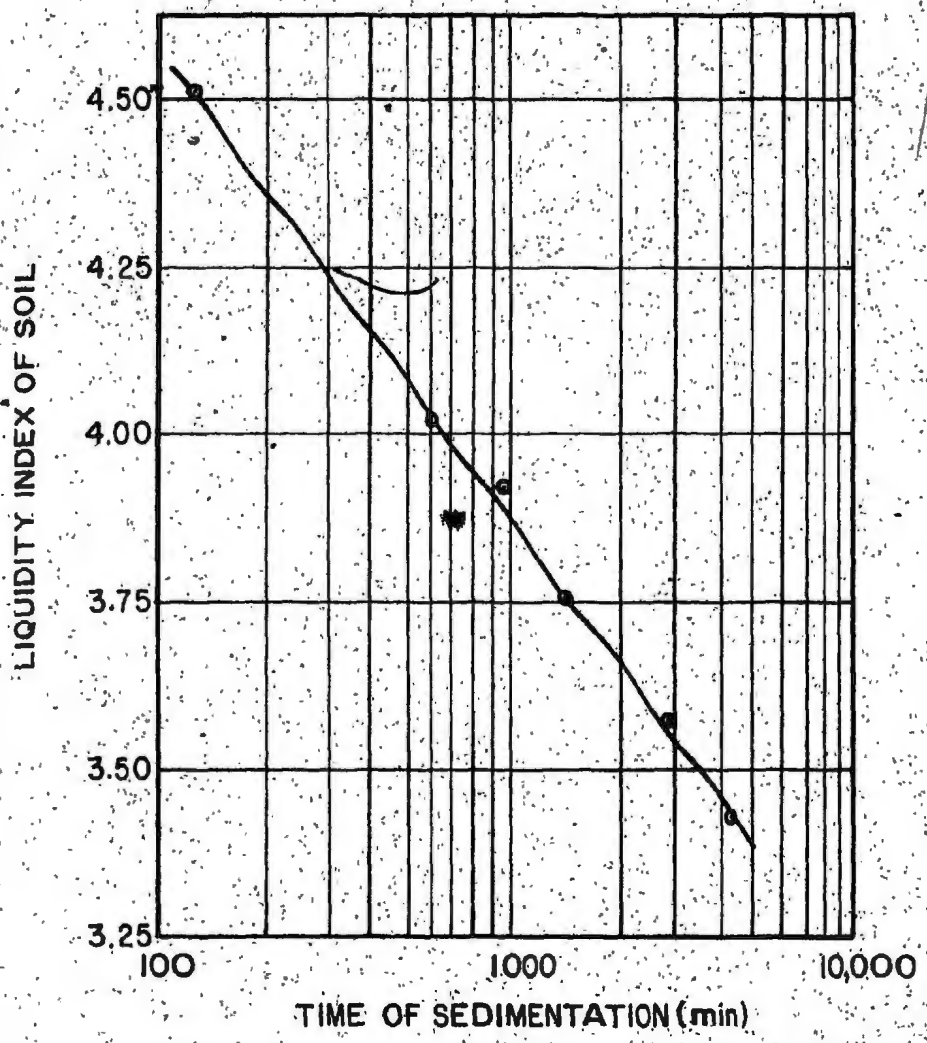

Fig. 15 LIQUIDITY INDEX VARIATION WITH TIME OF SEDIMENTATION

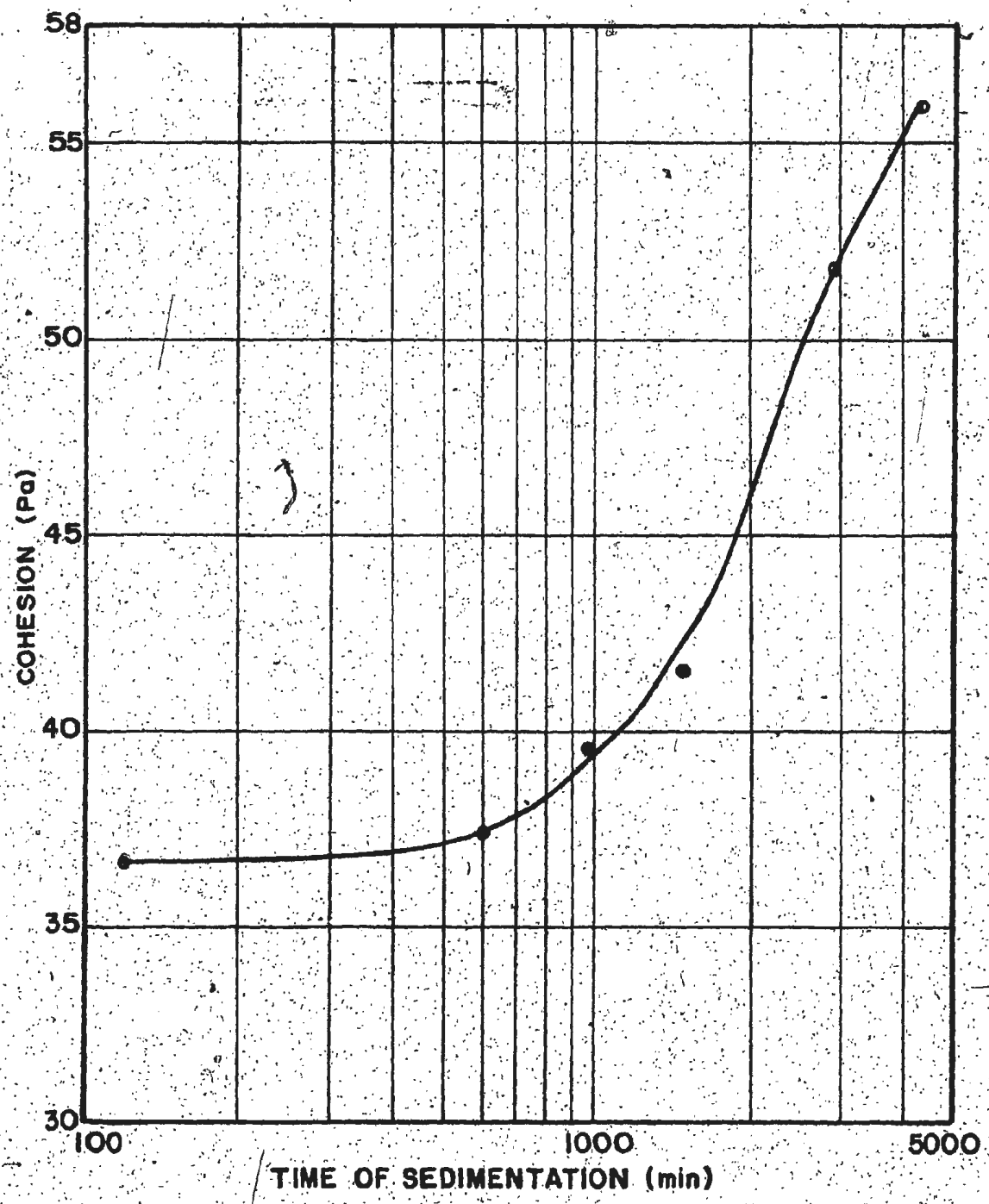

Fig. 16 TIME OF SEDIMENTATION VERSUS COHESION

the initial period of sedimentation. It is also noted that the gain in shear strength does not reach an equilibrium after the primary sedimentation period. Due to thixotropic effects (Terzaghi and Peck, 1967) and the subsequent molecular bonding of the clay minerals (Mitchell, 1976), the shear strength will continue to increase beyond the 72 hour primary sedimentation.

4.2.2 Comparison between adhesion (c_a) and cohesion ($\bar{c}$)

The unit adhesion c_a between the object and soil was computed as a ratio of the pull out load to the embedded area of the plate. The adhesion on the plate corresponding to zero time of sedimentation was ignored. The vane shear strength was measured at different points along the depth of object embedment, and averaged as the average cohesion $\bar{c}$.

The relationship between c_a and $\bar{c}$ for different materials is shown in Figure 17. It can be seen that the adhesion increases with cohesion for all materials and the rate of increase is slower at higher values of cohesion. Moreover, adhesion is also a function of surface roughness of the materials. At any value of the cohesion, adhesion is larger for rougher materials except for plexiglas and glass. The anomaly for plexiglas plate is attributed to the surface unevenness.

Plexiglas sheets are invariably not of constant thickness and not perfectly plane. Although from

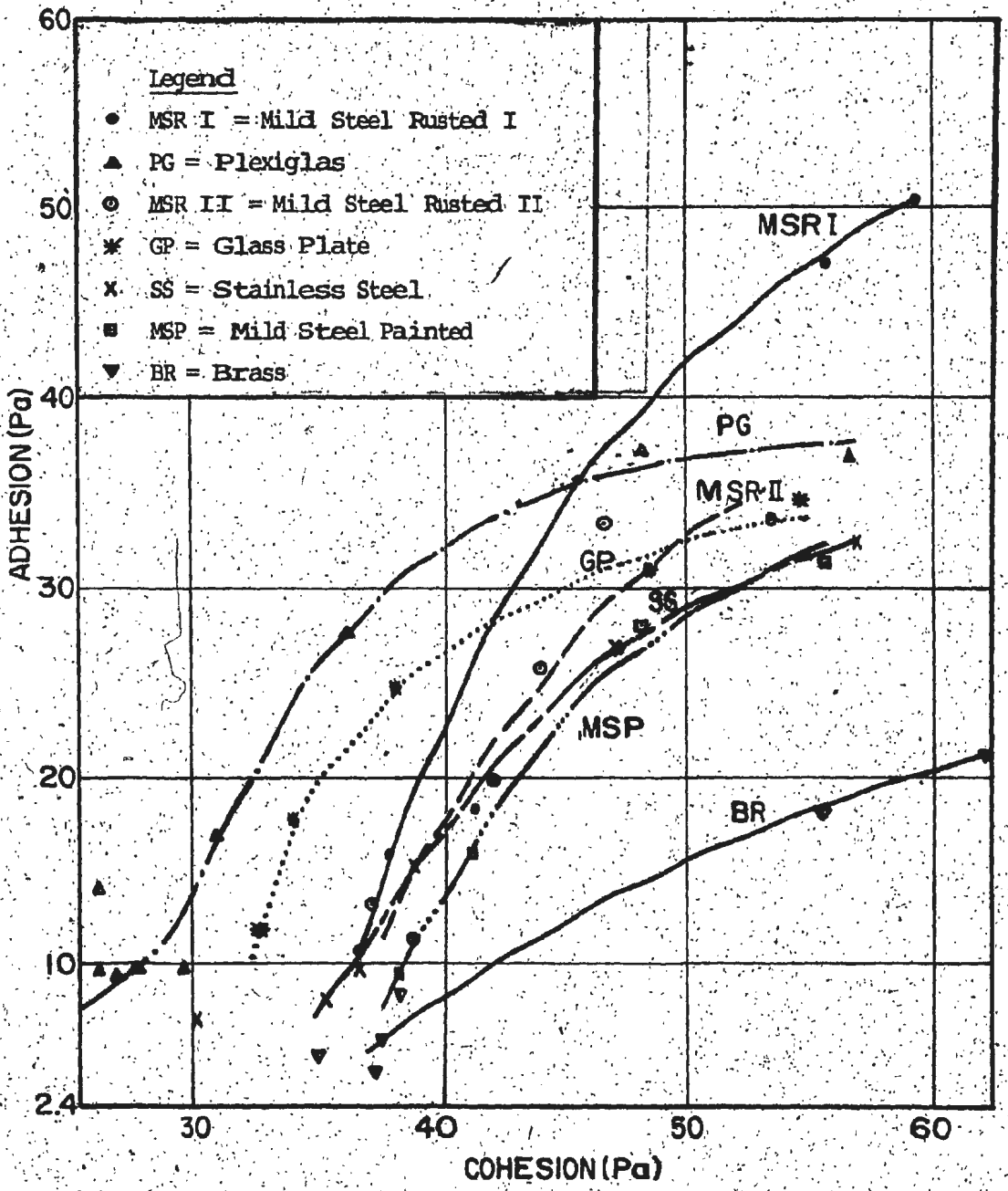

Fig. 17 RELATIONSHIP BETWEEN ADHESION ON PLATE MODELS AND COHESION OF THE SOIL

micro-roughness considerations, it can be classified as smooth, the surface has undulations. The sloping line of Figure 18b is a qualitative confirmation of the surface unevenness. When such a plate is pulled out of soil, the adhesion, at least in part, is between soil and soil rather than between soil and object. Figure 20 schematically explains this process and the anomaly of the results for plexiglas. Figures 18 and 19 also show the plot of surface roughness of all the other plate models.

In the case of glass sheets it is the physico-chemical action (Mitchell, 1976) causing the anomaly. When a glass plate is immersed in a soil slurry and the soil allowed to settle, molecular attraction takes place causing a strong silica bond between the molecules of clay minerals (mainly illite and kaolinite), quartz and the chemical constituents of glass (consisting mainly of silicates of potassium, calcium and sodium). The pull out load recorded in this case includes this force of molecular attraction along the soil-glass interface in addition to the normally understood soil adhesion. The above phenomenon can also be substantiated qualitatively since it is known that considerable force is necessary to slide two glass plates whose surfaces are free from impurities (cleaned with caustic soda solution), the coefficient of friction being close to unity (CRC Handbook of Materials Science, 1974). This is caused by the molecular reorientation and attraction

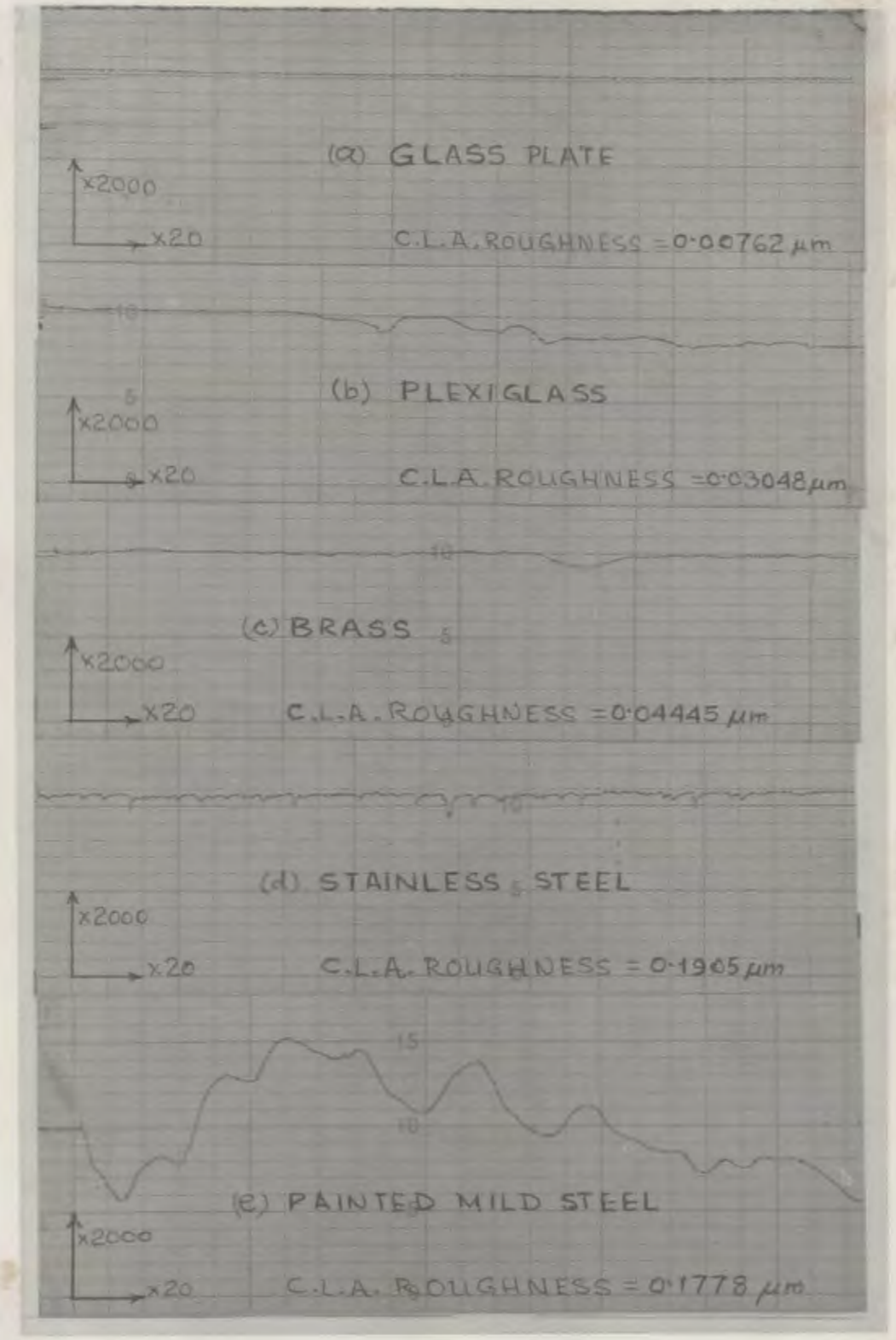

Fig. 18 SURFACE ROUGHNESS OF (a) GLASS PLATE, (b) PLEXIGLAS, (c) BRASS, (d) STAINLESS STEEL, and (e) PAINTED MILD STEEL PLATE MODELS

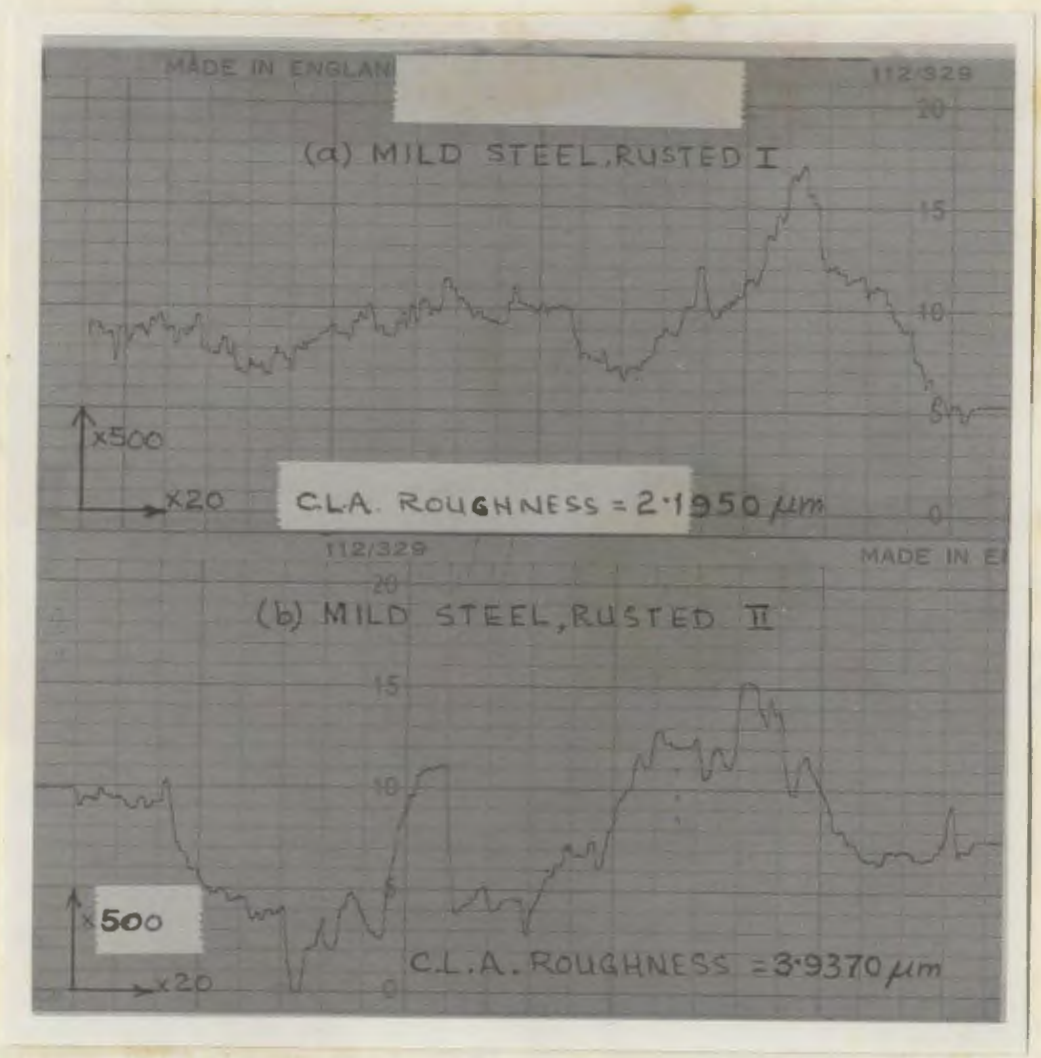

Fig. 19 SURFACE ROUGHNESS OF (a) MILD STEEL RUSTED I, and (b) MILD STEEL RUSTED II PLATE MODELS

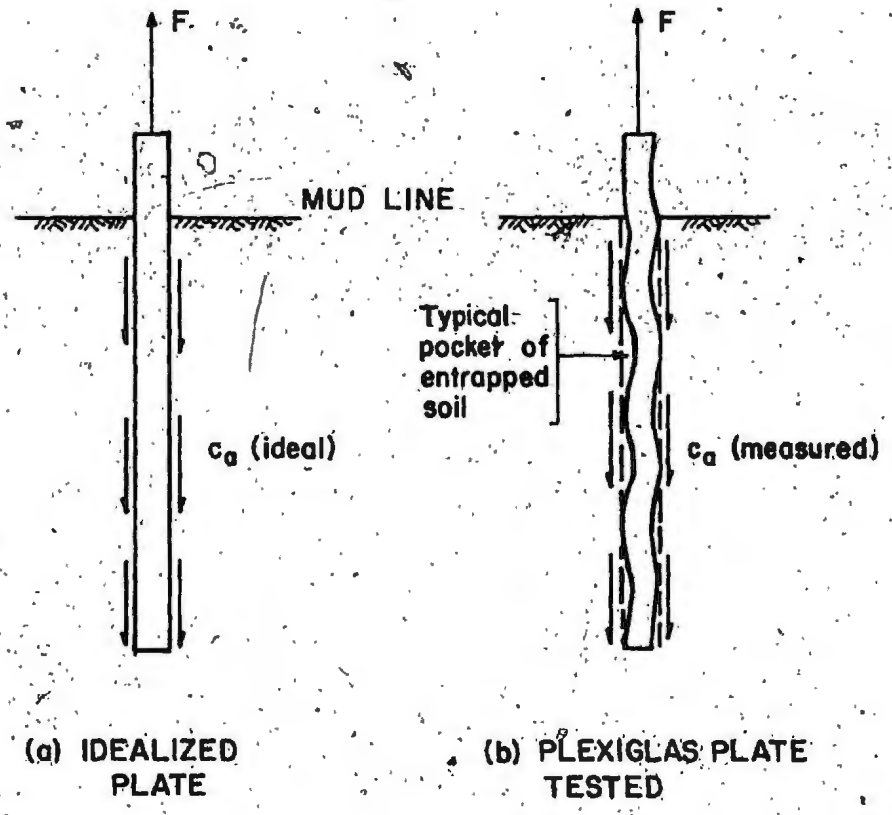

Fig. 20 CONCEPTUAL DIAGRAM SHOWING THE EFFECT OF SURFACE UNDULATIONS IN PLEXIGLAS PLATE MODEL

phenomenon between the molecules of two clean glass plates. A similar physico-chemical action between soil and glass is attributed to the increased adhesion in the case of glass, although its micro roughness is small.

4.2.3 Adhesion to surface roughness relationship

The ratio of adhesion to cohesion is designated by α, the adhesion ratio. This ratio for the various materials at different periods of sedimentation is shown in Figure 21. Table III summarizes the values of surface roughness as measured by Taylor-Hobson No. 4 Talysurf, and expressed as center line average in microns (μm) over a cut-off length of 0.254 mm. α increases with increase in surface roughness, except for the anomaly in the case of glass and plexiglas, which has already been explained.

Figure 21 also shows that α for stainless steel and painted mild steel plates are very close to each other as also are their roughness values (Table III). Comparison of the results obtained for only the metal plates shows that the higher the roughness value, the higher the value of α (Fig. 21A). This indicates that for all types of metal plates, α is a function of the surface roughness.

4.2.4 α as a function of cohesion

The relationship between α for the different models and soil cohesion, is shown in Figure 22. It can be seen that α increases with cohesion for all materials. However,

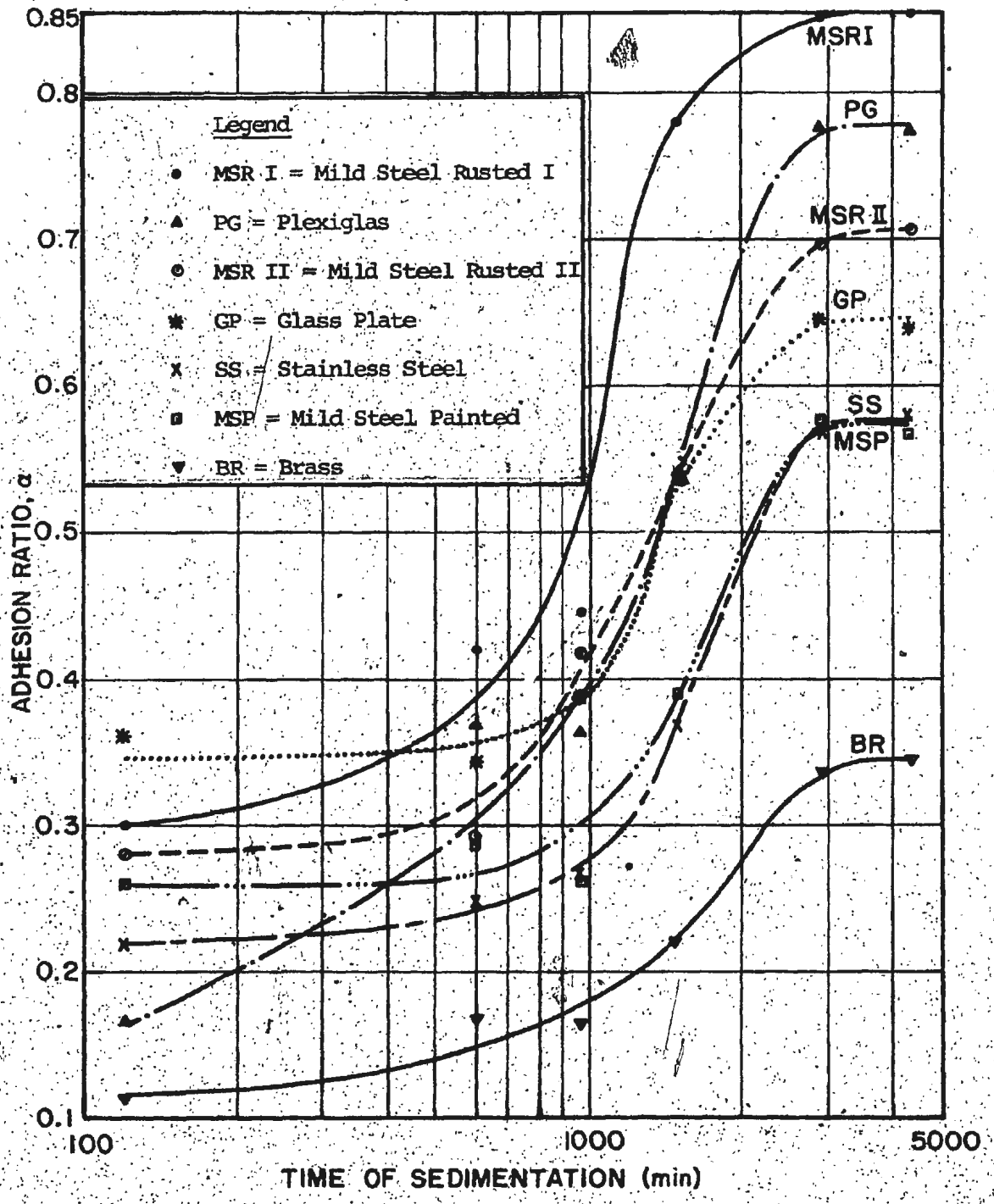

Fig. 21 RELATIONSHIP BETWEEN α AND TIME OF SEDIMENTATION

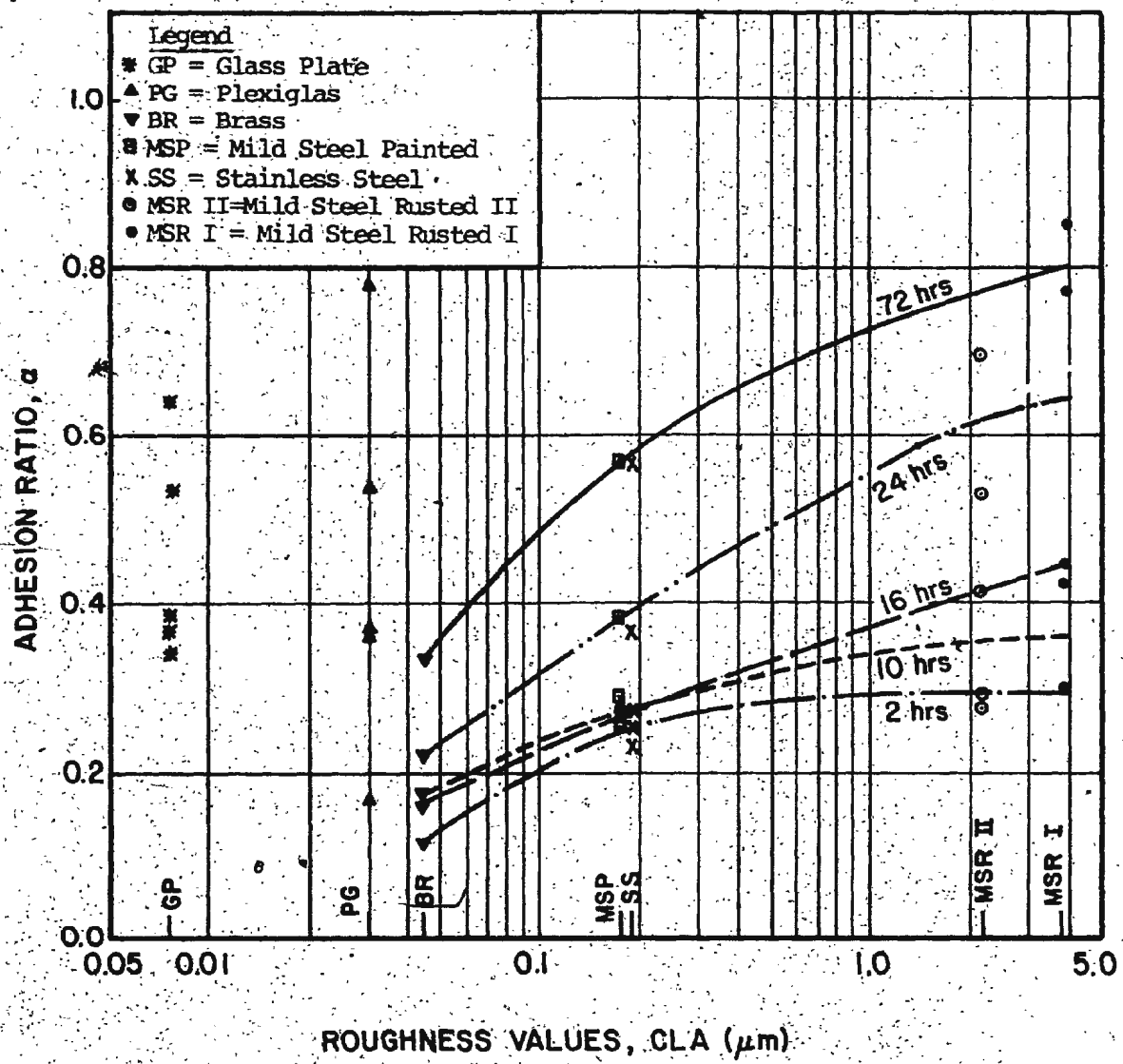

Fig. 21A SURFACE ROUGHNESS - α RELATIONSHIP

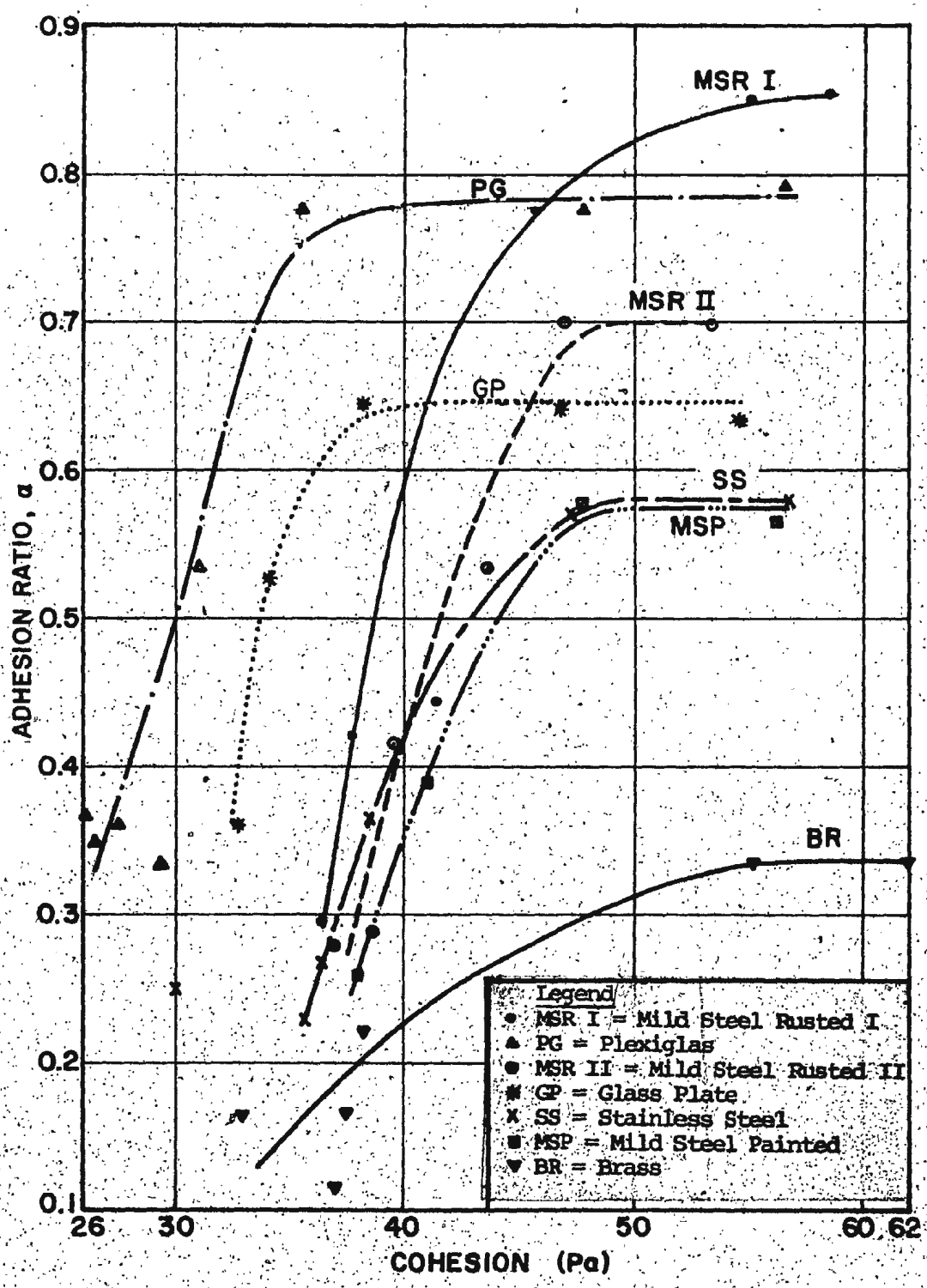

Fig. 22 α AS A FUNCTION OF COHESION FOR PLATE MODELS

the rate of increase reduces at higher cohesion values. At any given value of cohesion, α is generally higher for materials with greater roughness except in the case of plexiglas and glass plate models. For a given material, the lesser the value of cohesion, the smaller is the value of α. The variation in the rate of change in α implies that the adhesion is not always a fixed proportion of cohesion, but varies non-linearly with the basic cohesion itself. For the soil used, beyond a cohesion value of 50 Pa, the value of α is constant, implying that adhesion will be directly proportional to $\bar{c}$ beyond this value.

4.2.5 Variation of α with percent sedimentation

Figure 23 shows the variation of α with percent sedimentation. The percentage of sedimentation is defined with respect to the standard 72 hours, which is the hypothetical 100% sedimentation. It is seen that α increases slowly during the initial 16 hour period of sedimentation and rapidly thereafter, before levelling off towards the end of sedimentation. The cohesion value also increases in a similar pattern (Figure 16) after the initial period of sedimentation. Comparison of Figure 16 and Figure 23 suggests that the rate of increase of the adhesion is faster than the basic soil strength in the initial stages. This effect could also be seen in Figure 17.

The percentage of sedimentation is shown alongside the time of sedimentation in Figure 23. About 72 percent of sedimentation takes place in the first 16 hours whereas

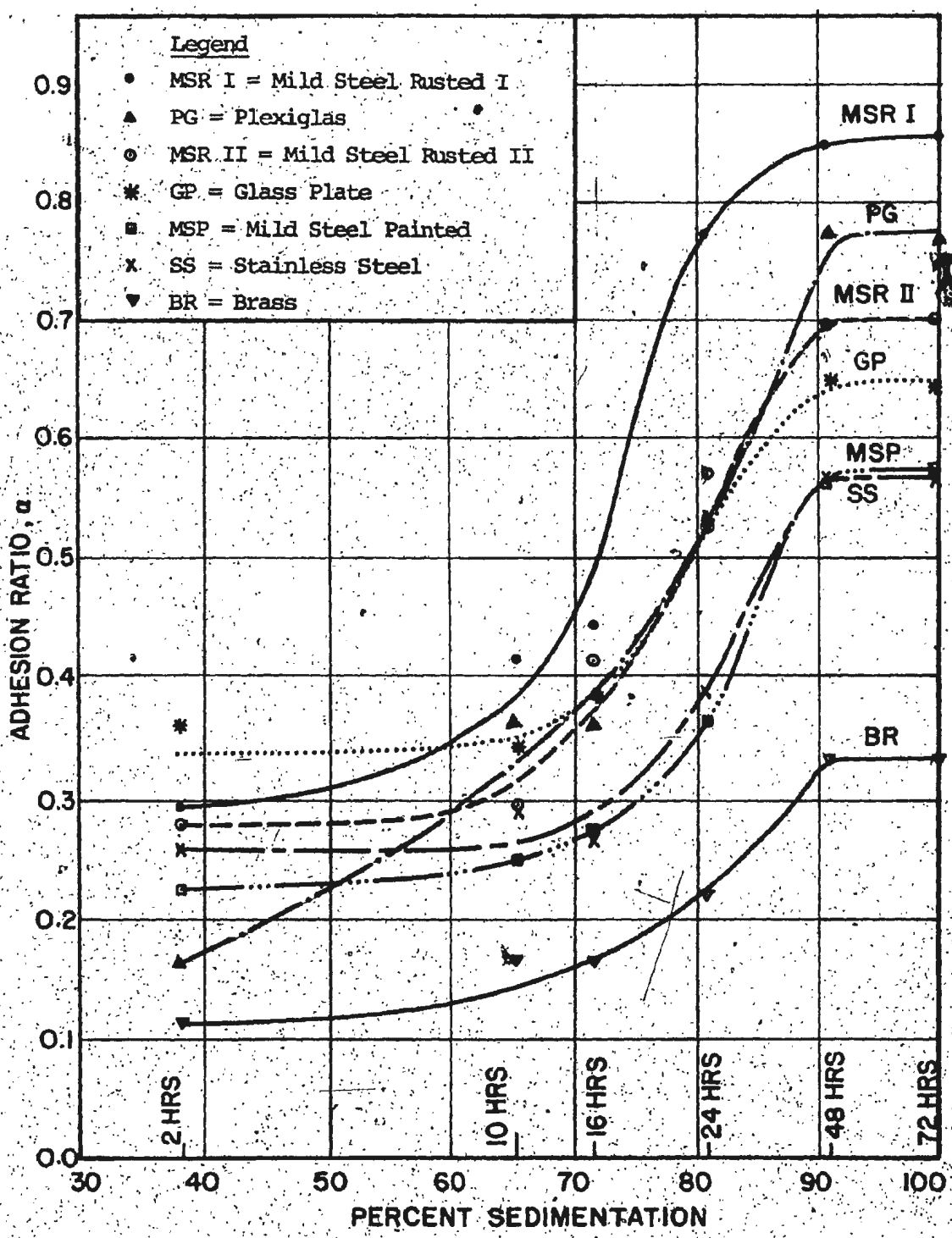

Fig. 23 VARIATION OF α WITH PERCENT SEDIMENTATION

only 20 percent further sedimentation takes place in the next 32 hours. In spite of a smaller rate of sedimentation between 16 and 48 hours the faster rate of increase of cohesion during this period influences the value of α.

4.2.6 Percent gain in α for different plate models

The value of α at 72 hours was taken as the standard reference α_{max} and the other intermediate α values for different lower sedimentation times were expressed as a percentage of the standard α_{max}. Results are presented in Figure 24. It is seen that the rate of change in α is similar for all plate models, slower during the initial period and rapid thereafter. Regardless of the type of material, the maximum increase in α is between 16 and 32 hours as already observed.

4.2.7 Influence of average unit weight of soil on α

The variation of α with average unit weight of soil is shown in Figure 25. For all plate models α increases with unit weight of soil. The increase in α is larger for plate models of higher roughness during the intermediate stage of sedimentation. At higher values of unit weights the value of α reaches an equilibrium, indicating a proportionally equal rate of increase of both adhesion and cohesion.

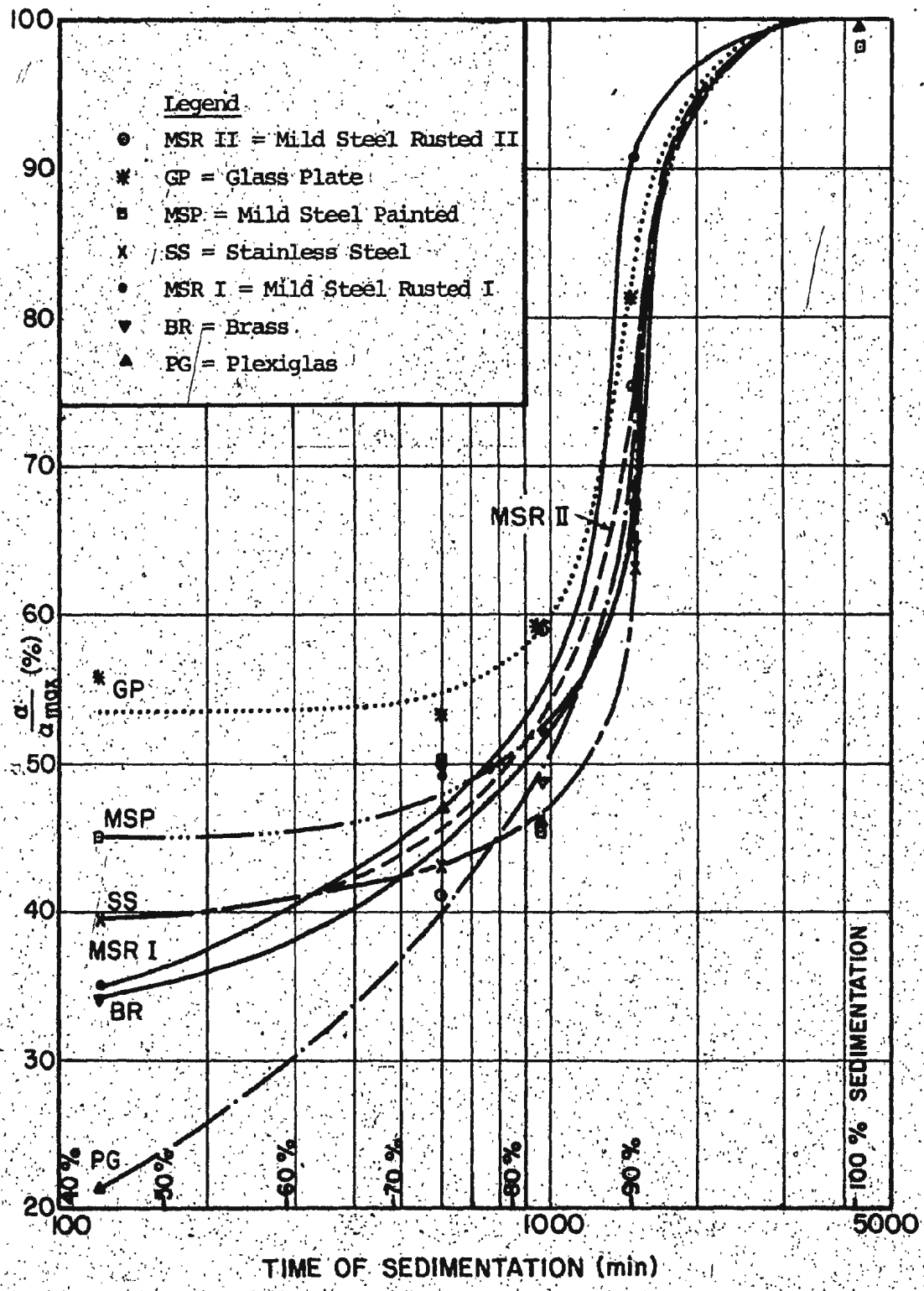

Fig. 24 PERCENT GAIN IN α VERSUS TIME OF SEDIMENTATION

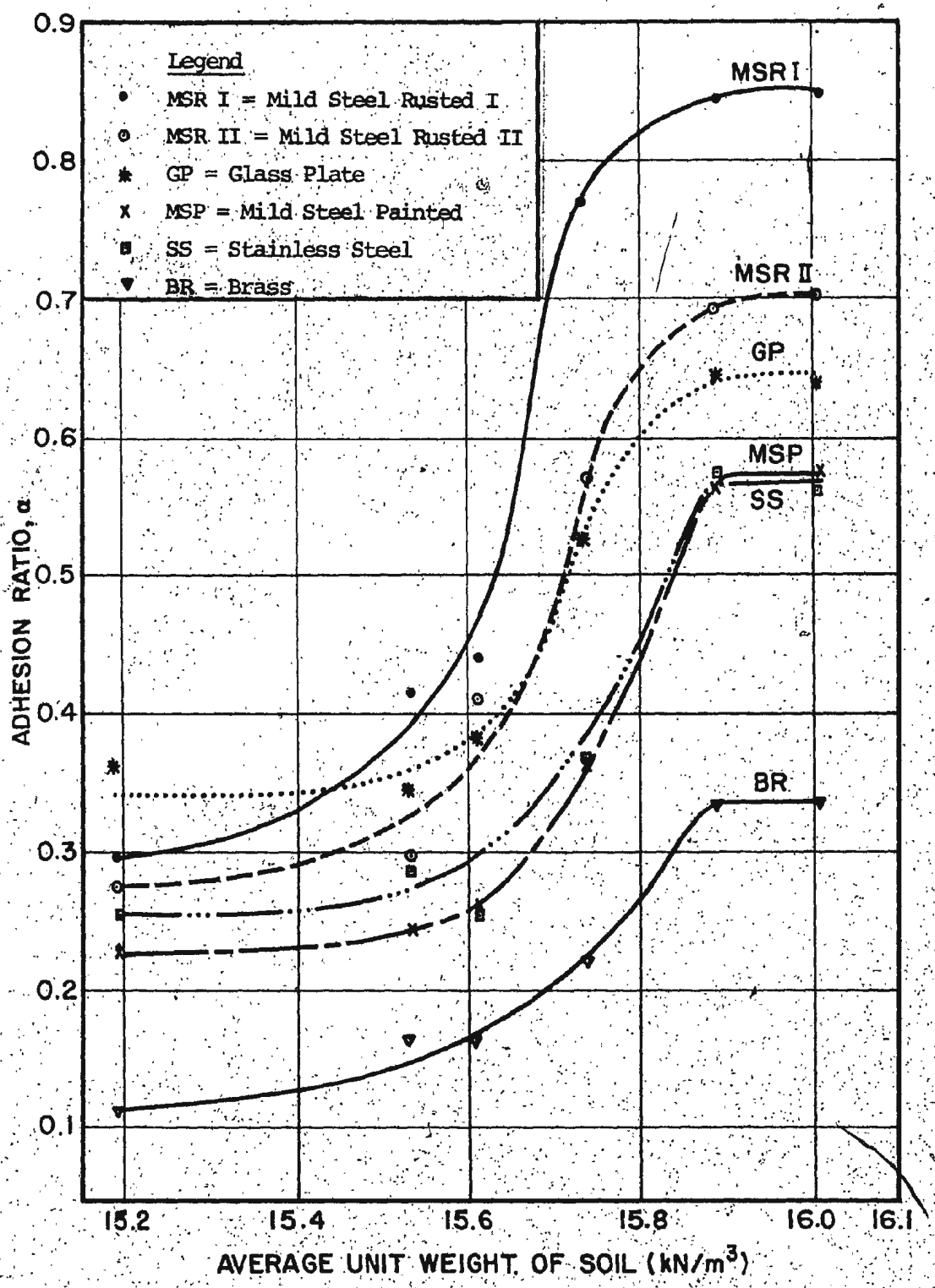

Fig. 25 VARIATION OF α WITH AVERAGE UNIT WEIGHT OF SOIL

4.2.8 α versus liquidity index of the soil

The relationship between α and the liquidity index of soil is presented in Figure 26. It shows that α increases with decreasing liquidity index (i.e., lower water content) for all the models tested. The increase in α value is slow at higher liquidity indices corresponding to initial periods of sedimentation. α increases rather rapidly at intermediate values of liquidity index in the order of 4.25 to 3.6. The increase in α is not very significant below a liquidity index of 3.6. α values are higher for models of higher surface roughness for a given value of the liquidity index. The α values obtained for plexiglas and glass plates are, however, high and the anomaly was explained earlier.

Figures 23, 25 and 26 are similar, leading one to conclude that the primary period of sedimentation and the period in which the soil reaches a state of nearly constant density is the factor influencing the values of α, for a given embedded object.

4.2.9 Effect of depth on cohesion, adhesion and the parameter α

The results so far discussed are based on the values of cohesion and adhesion averaged over the depth of embedment of plate models. The value of cohesion itself varies with the depth below the soil surface. For a 24 hour sedimentation, the values of adhesion at four different depths were obtained by embedding the plate to that depth. Stainless steel plate

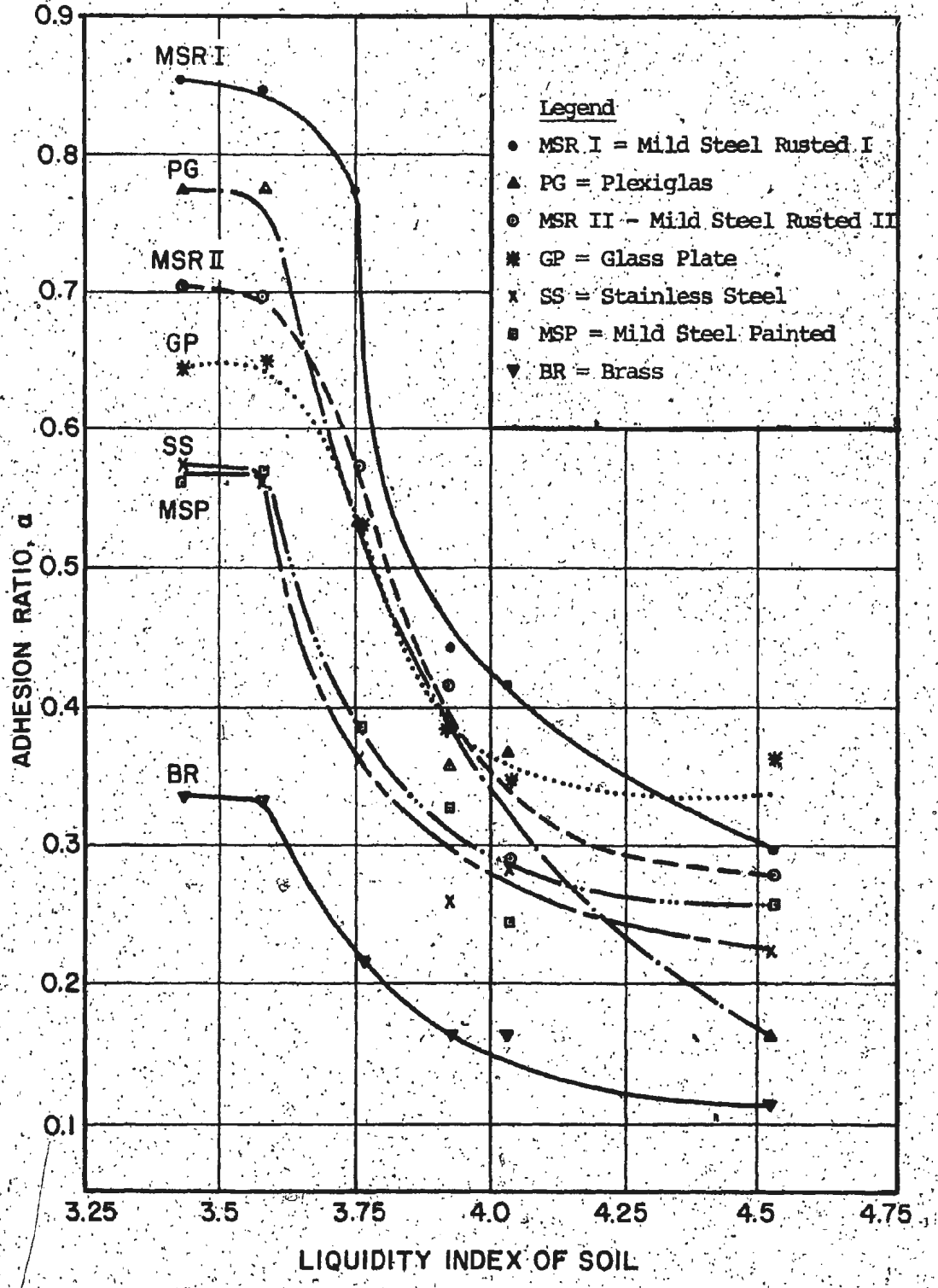

Fig. 26 α VERSUS LIQUIDITY INDEX OF SOIL

model was used in these tests. Corresponding value of cohesion at that depth was also measured. The results are summarized in Figure 27. Similar results would be expected for other plate models as well.

It can be seen that the cohesion increases with depth and so also the adhesion. The ratio α also follows the same pattern. For the range of depth studied, the values of α increase with increase in the average cohesion. This effect of depth was not taken into account in the interpretation of Figures 21 to 26, in which values of c, c_a and α were averaged. It is also to be noted that the depth of embedment was kept constant in all the tests so that the comparison of averaged results becomes meaningful.

These results are significant in that one has to use caution in averaging the cohesion, particularly in the calculation of pull out forces for objects which are deeply embedded.

4.3 Results on Ice Sheet Tests

The experimental results on the adhesion between soil and fresh water ice sheets are presented and discussed below.

4.3.1 Variation of unit adhesion with cohesion

The average cohesion over the embedment depth was calculated, based on cohesion values at different depths, and plotted against unit adhesion as shown in Figure 28. The adhesion is seen to increase uniformly with cohesion. The soil, in these tests, did not gain a strength comparable to those of the plate model tests. The presence of the antifreeze with a high specific gravity (1. 14) is the reason attributed for this phenomenon. Use of sea water at the operating temperature of $-3^{\circ}C$ of the cold room caused the freezing of the soil itself and hence was not attempted

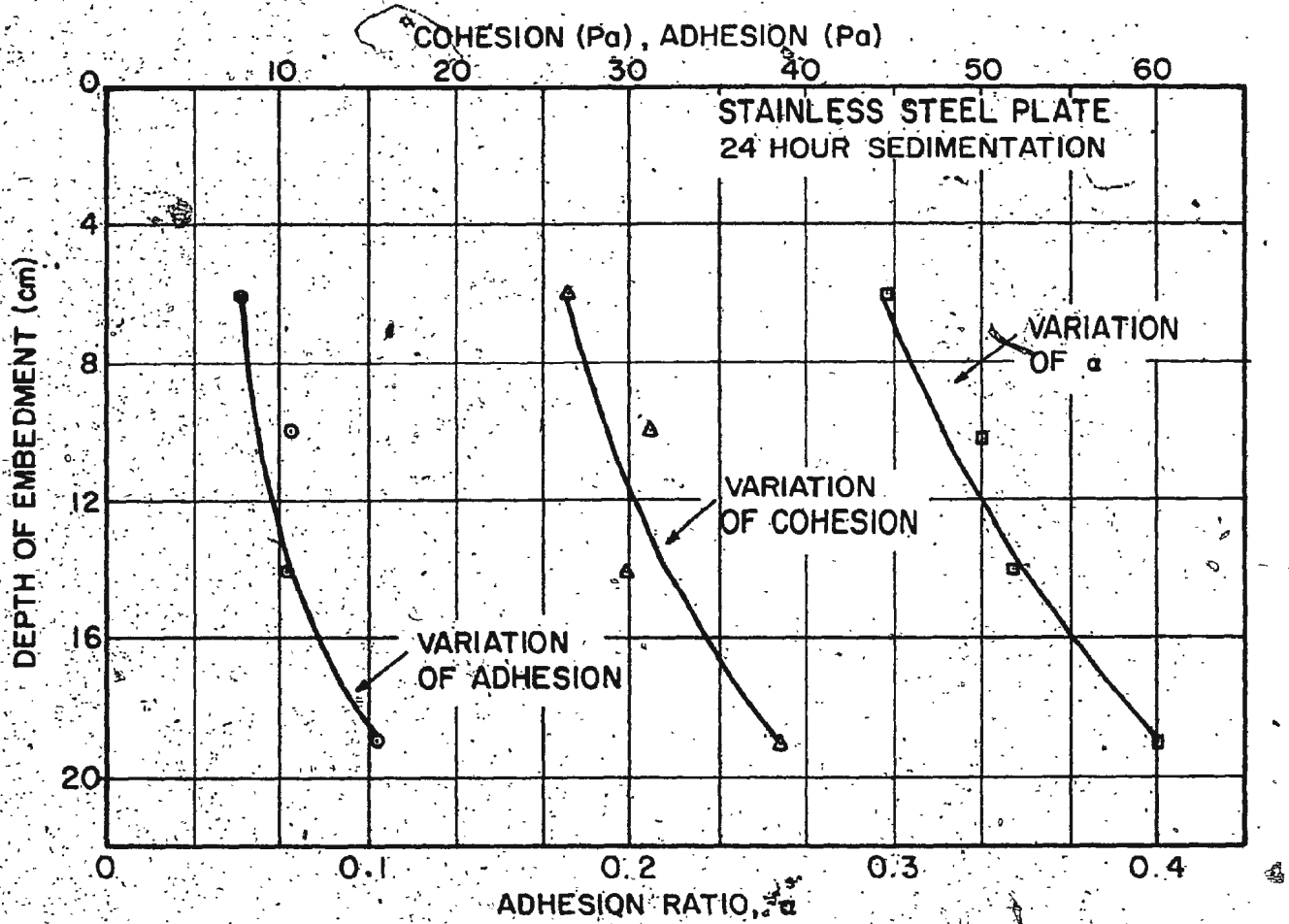

Fig. 27 VARIATION OF COHESION, ADHESION AND PARAMETER α WITH DEPTH OF EMBEDMENT FOR STAINLESS STEEL PLATE MODEL AT 24-HOUR SEDIMENTATION

further.

4.3.2 Relationship between α and time of sedimentation

The α - sedimentation time relationship for ice sheet is presented in Figure 29. The increase in α with time, does not appear to be significant (from 0.63 to 0.66). The presence of a film of melt water around the embedded portion of ice sheet caused by the presence of antifreeze might result in an almost constant value of α in the range of cohesion values studied (Figure 28). Secondly, the presence of antifreeze caused pitting of the ice sheet. The value of α is in the order of 0.65 which is somewhat high considering the fact that the ice surface is smooth. This is an experimental inadequacy which has to be considered in interpreting the results of the tests with ice sheet. It is probable that one would notice a similar pitting phenomenon in the ocean environment, at the ice-soil contact, together with a film of melt water at the interface. In such a case, α value is likely to be in the range of 0.65. No other meaningful conclusion can be drawn at this stage from the laboratory tests.

4.4 Partially Embedded Plexiglas Prismatic Models

The pull out resistance of a prismatic object partially embedded in a cohesive soil can be written as

$$P = \alpha.\bar{c}.A + p_s.A_b \qquad [7]$$

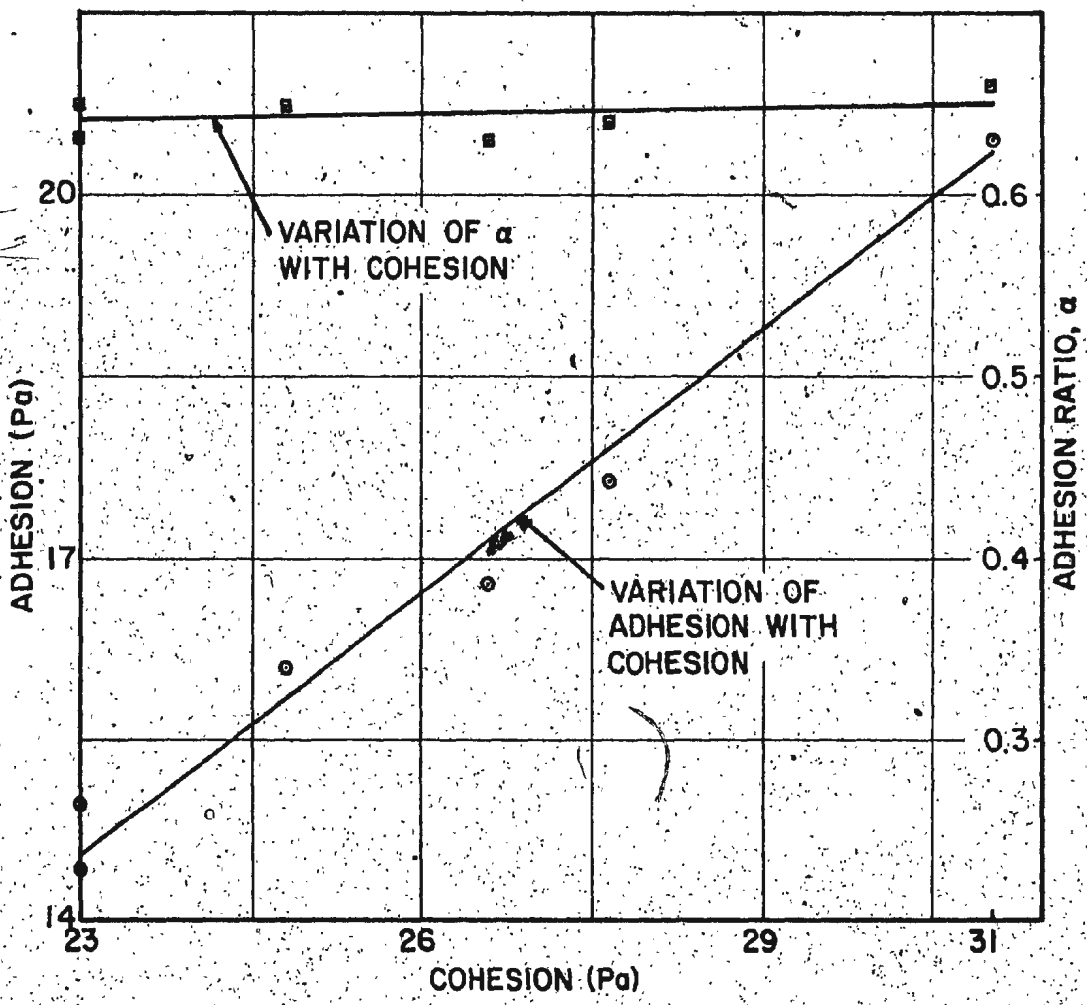

Fig. 28 VARIATION OF UNIT ADHESION AND α WITH COHESION FOR ICE SHEET TESTS

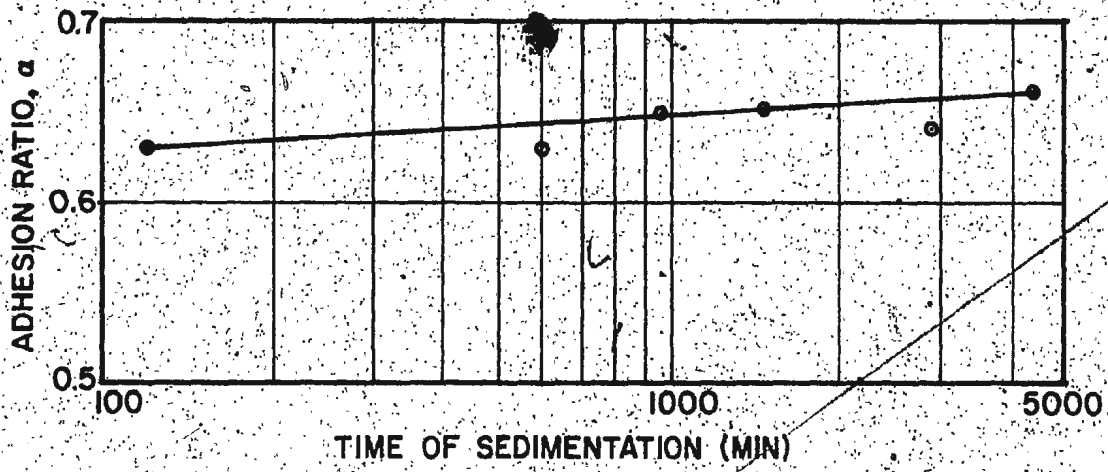

Fig. 29 α-TIME OF SEDIMENTATION RELATIONSHIP FOR ICE SHEET TESTS

where

P = pull out load

α = adhesion-cohesion ratio

$\bar{c}$ = average cohesion along the embedment depth

A = vertical surface area of the object in contact with soil

p_s = unit base suction

A_b = projected area of the base of the object.

The value of $\alpha.\bar{c}.A$ includes the initial adhesion C_{ia}, on vertical object-soil interface at the time of embedment of object (at time of sedimentation = 0). However, the value of C_{ia} is very small, and hence neglected. The unit base suction can be expressed as:

$$p_s = \beta . c_b \qquad [8]$$

where

β = a dimensionless parameter, and

c_b = cohesion at base level of the object

From equations [7] and [8], β can be written as

$$\beta = \frac{1}{A_b . c_b} . [P - \alpha . \bar{c} . A] \qquad [9]$$

The parameter β is similar to the dimensionless co-efficient, F_u, in equation [6].

The depth of embedment of these models was the same as that for plate tests. Hence the values of α as obtained from plate tests can be used in equation [9].

4.4.1 Influence of bottom profile on unit base suction

Experiments for determining base suction were carried out using plexiglas prismatic models of various base configurations, i.e., flat base, pyramidal base with apex angles 90° and 135°, and flat base with all round skirt, 5 cm. high. All these models were 7.62 cm. x 7.62 cm. square in plan, and 22.5 cm. long.

Figure 30 shows the relation between cohesion and unit base suction for these models. The base suction-cohesion relationship is linear except at low values of cohesion. In the case of objects with a flat or projecting base, the base resistance appears to be dependent only on the projected horizontal area. Base suction is almost the same for all the models except for the model with an all round skirt. The presence of skirt all around the flat base increases the base suction significantly. The factor contributing to this increased base suction is most likely to be the soil to soil interaction between the wedge of soil entrapped within the skirt zone and the soil outside at tip level of the skirt.

4.4.2 Relationship between liquidity index and parameter β

Figure 31 shows the variation of β with liquidity index. It is seen from this figure that β increases linearly with decrease in liquidity index. For the values of liquidity index of these experiments, β appears to be independent of the shape of the base except for the model with all round skirt. During the initial stage of sedimentation β increases very slowly with decrease in liquidity

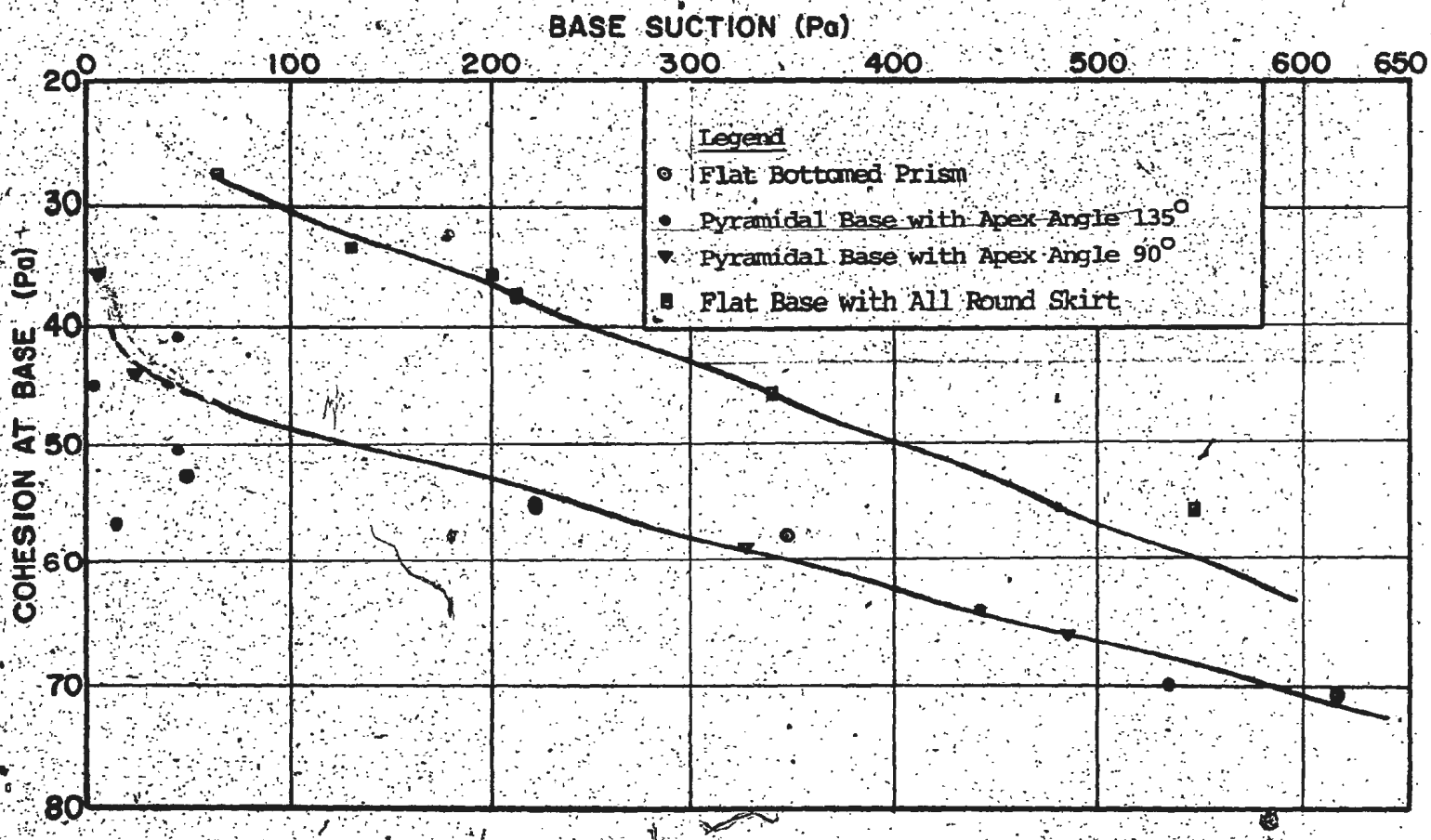

Fig. 30 BASE SUCTION AS A FUNCTION OF SEDIMENT STRENGTH FOR PLEXIGLAS PRISMATIC MODELS OF SQUARE CROSS-SECTION

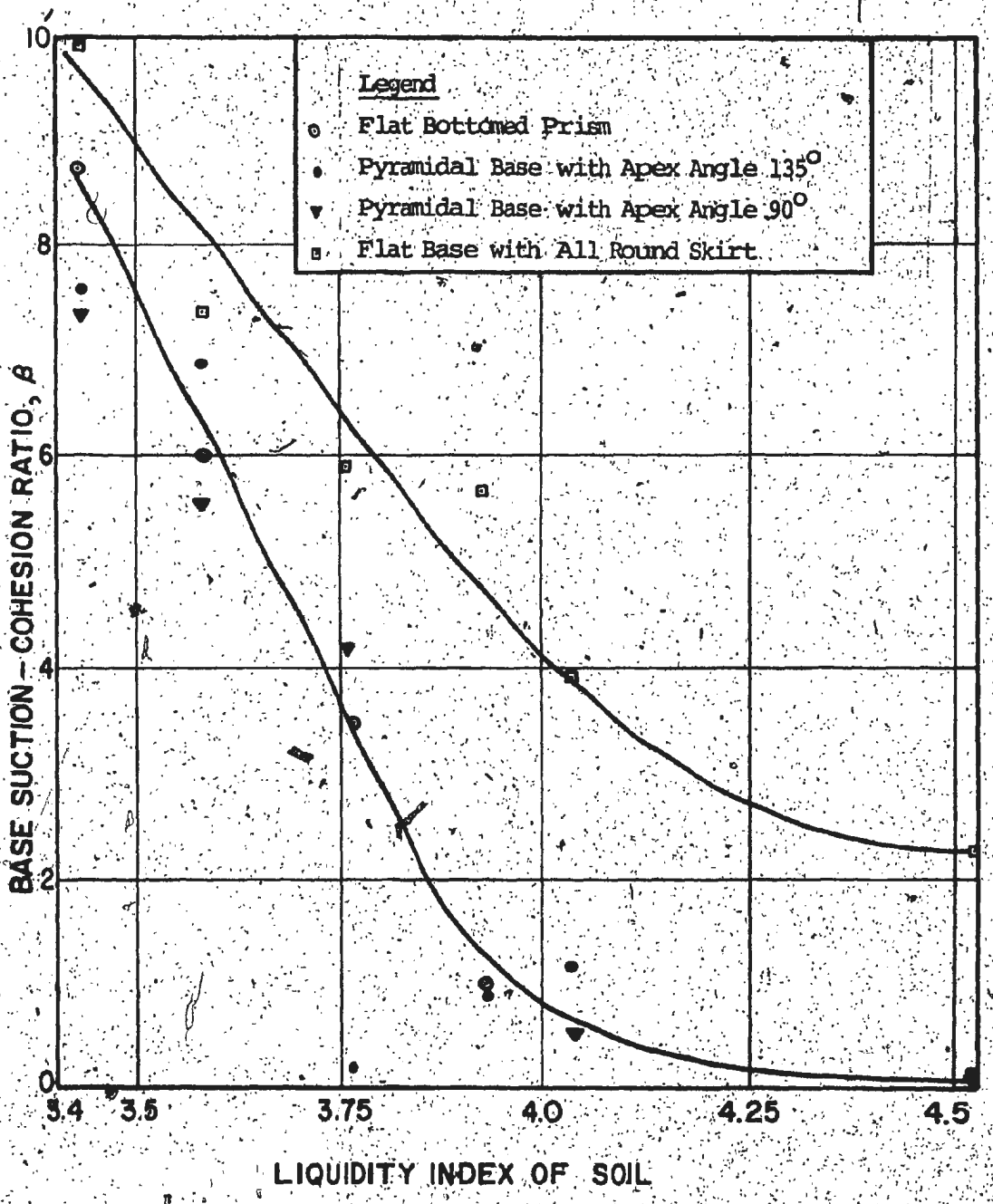

Fig. 31 VARIATION OF BASE SUCTION-COHESION RATIO WITH LIQUIDITY INDEX OF SOIL

index. The range of β for all the tests was from 0.1 to 10, while the liquidity index varied between 3.4 and 4.5, and the corresponding cohesion at the base varied from 20 Pa to 70 Pa. It may be recalled that the parameter α, too, increases rapidly for values of liquidity index less than 4 as shown in Figure 26.

The variation of β for the model with a skirt around the base is similar to that for the other models. However, the absolute values of β are higher for this case for any given value of the liquidity index. This is in conformity with the conclusions in para. 4.4.1.

4.4.3 Variation of β with depth to breadth ratio (D/B)

The ratio of the least lateral dimension B and the depth D is an important factor which influences the behavior of any foundation in soils and its bearing capacity. The problem of pull out has sometimes been termed the problem of "reverse bearing capacity" and theoretical formulation has been proposed by Lee (1972). To verify the effect of D/B ratio on the pull out and also to compare the results with the available theoretical formula, the plexiglas models were partially embedded to different depths and the value of β determined in each case.

Results were obtained from tests with 48 hours sedimentation for the models with flat as well as pyramidal base of apex angles 90^{o} and 135^{o} and plotted in Figure 32. A comparison of the β values obtained from the semi-empirical formula of Lee (1972) is shown in Figure 32. Breakout of fully embedded objects has sometimes been

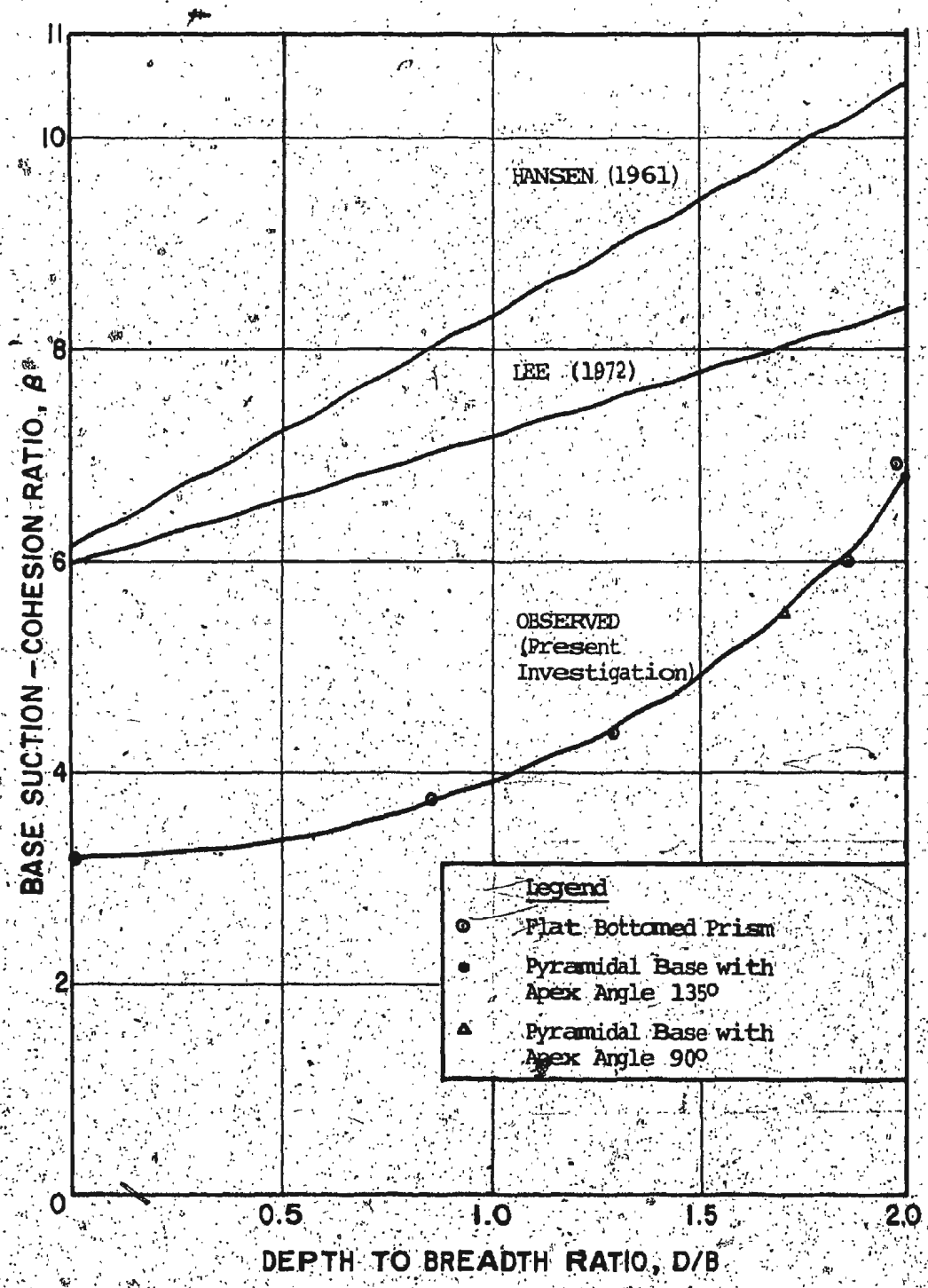

Fig. 32 COMPARISON OF UPLIFT RESISTANCE, PREDICTED FROM BEARING CAPACITY THEORIES, WITH OBSERVED BASE SUCTION

directly compared to the bearing capacity problem (Byrne and Finn, 1978) with appropriate corrections for depth, eccentricity, shape and inclination of the load as given by Hansen (1961). Such a comparison is made for the experiments conducted in this study and also shown in Figure 32. At the surface, where D/B value is zero, β was found to be about 3. The values of β increase with increasing D/B ratio. Lee (1972) has given an analysis for immediate breakout of partially embedded objects and draws analogy to the bearing capacity problem. It has been established by semi-empirical formula that values of β increase with increasing D/B ratio, which is confirmed by the present experiments. However, the variation is not linear as suggested by the theoretical equations. It is also observed that the values of β obtained by theoretical equations are higher than those obtained experimentally. The theoretical formulations contemplate a soil in which a general bearing capacity failure takes place. Such a failure is not likely to occur in very loose soils in which punching shear is more likely (Vesic, 1973). Most of the discrepancy between the experimental and theoretical values is attributed to the soil property which is far different from that contemplated in the theory. The reverse bearing capacity formula and Hansen's (1961) equation overestimate the β values by a factor of about 2 for the range of D/B ratio tested and for the type of soil used in the present investigation. Figure 32 also shows that the apex

angle of the pyramidal base has no significant influence on β.

The values of β obtained from the present tests and those obtained from shallow anchor uplift theories, as well as the experiments on horizontal anchor plates by Davie and Sutherland (1977) are presented in Figure 33. It can be seen from Figure 33 that uplift theories also overestimate values for D/B greater than about 1.0, whereas the experimental values of Davie and Sutherland are smaller than the values obtained from present investigation for any D/B value.

The comparisons in Figures 32 and 33 are to be qualified by the fact that the method of sample preparation reported here are not identical to those of the other authors. However, since the breakout phenomenon is the same, a correlation of the different results is appropriate.

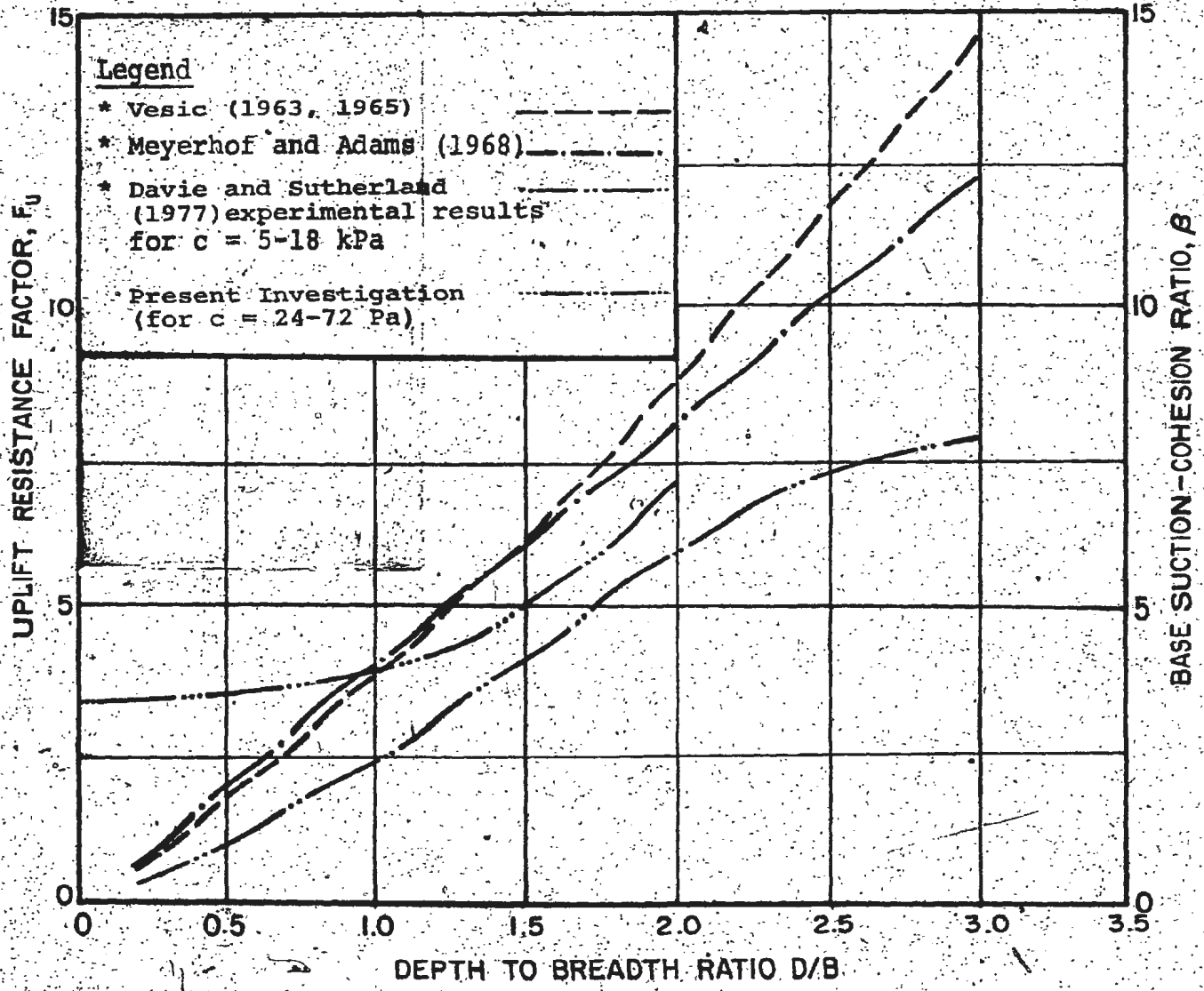

Fig. 33 COMPARISON OF UPLIFT RESISTANCE FACTOR, F_u, PREDICTED FROM SHALLOW ANCHOR UPLIFT THEORIES, WITH OBSERVED BASE SUCTION-COHESION RATIO, β (* as reported by Davie and Sutherland 1977)

4.5 Fully Embedded Plexiglas Models of Different Shape

The evaluation of breakout force for fully embedded objects includes two additional factors besides the parameters α and β. These are the shearing resistance of the soil mass above the embedded object and the vertical component of the adhesion on the top surface. Figure 34 shows the forces acting on fully embedded objects, of different shapes. At the onset of breakout, the soil mass above the embedded object has to fail. The type of failure depends on the type of soil. While evaluating the types of bearing capacity failures, Vesic (1973) classified these as punching shear for highly compressible soils, general shear for relatively incompressible soils and local shear for soils in between. By a similar analogy during pull out of fully embedded objects from very weak and compressible soils such as that used here, punching shear failure can be assumed to take place with vertical slip surfaces. Figure 34 gives a break-up of the various forces at the onset of breakout for fully embedded objects, immediately after the object is embedded, and after a time t. Since the weight of the object was counterbalanced in the actual experiments, the difference between the two expressions [10] and [11] of Figure 34 is the theoretical breakout force for the laboratory conditions. The breakout force P will therefore be:

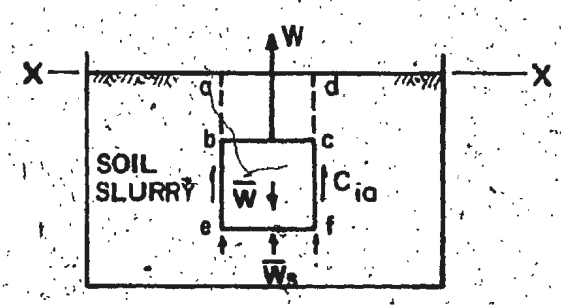

(i)

AT TIME, T=O

x-x: Soil slurry level

W: Counter balancing load

$\bar{W}$: Weight of the object in air

$\bar{W}_s$: Soil buoyancy

$(\bar{W}-\bar{W}_s)$: Effective weight of the object in slurry

For equilibrium of the system at T=0,

$$W = (\bar{W} - \bar{W}_s) - C_{ia} \qquad [10]$$

where C_{ia} = initial adhesion during embedment

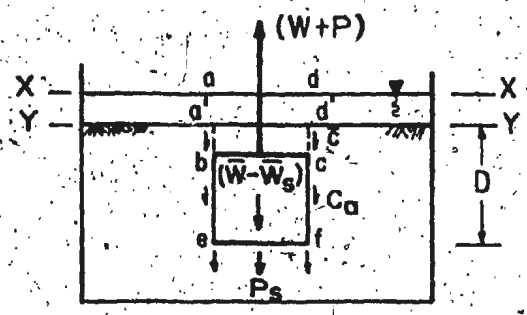

(ii)

AT THE ONSET OF BREAKOUT

(FOR OBJECTS WITH FLAT TOP)

At the onset of breakout,

$(W + P) = (\bar{W} - \bar{W}_s)$ + [cohesion along vertical failure plane, a'bcd'] + [adhesion along vertical object-soil interface] + [Base suction, P_s] + [Vertical component of adhesion, C_{ta}, for objects with curved top [11]

Where, P = Additional load to Breakout

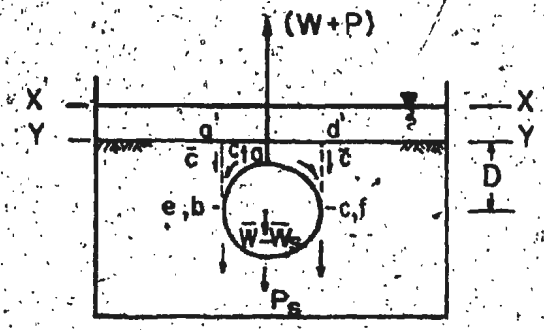

(iii)

AT THE ONSET OF BREAKOUT

(FOR OBJECTS WITH CURVED TOP)

Fig. 34 FORCES CONSIDERED IN THE BREAKOUT OF FULLY EMBEDDED OBJECTS

P = Initial adhesion at T = 0.

+ cohesion along soil failure surface

+ adhesion along vertical soil-object interface

+ base suction at object bottom

+ vertical component of adhesion on the top curved surface of the object [12]

Breakout load was determined for two different depths of embedment. Table IV gives the comparison between the theoretical breakout loads, as obtained by eq. [12], and the experimental values. There is a reasonably good correlation between the computed and observed loads. The difference between the observed and theoretical values would be even less, if a curved failure surface is assumed, instead of the vertical failure planes. It may be noted that only the projected area of the base is considered for computing the base suction in the case of a right circular cylindrical object with longitudinal axis horizontal and also in the case of a sphere. A similar approach was made by Müga (1968) and the correlations reported to be satisfactory.

There is also a good correspondence between the breakout forces on sphere and hemisphere at comparable $\frac{D}{B}$ values indicating that the base configuration has no significant effect on the base suction. A similar conclusion was drawn earlier in the case of partially embedded objects of different base configurations.

TABLE IV

COMPARISON OF OBSERVED BREAKOUT LOADS WITH THE VALUES OBTAINED USING PARAMETER α AND β FOR FULLY EMBEDDED OBJECTS*

Shape and Type of Embedded Object	D/B Ratio	Base-Suction Force, P_s (N)	Adhesion on Top Curved Surface, C_{ta} (N)	Adhesive Resistance on Sides, C_a (N)	Cohesive Resistance Along Soil Failure Plane, C_{AB} (N)	Total Breakout Load, $P = P_s + C_{ta} + C_a + C_{AB}$ (N)	Observed Breakout Load (N).
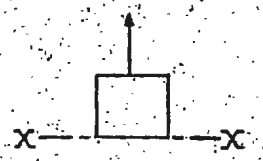 Cube, 7.92 cm Side	2.033	2.19		0.99	1.29	4.47	4.22
	1.53	1.58		0.97	0.68	3.23	2.94
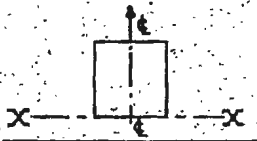 Rt.Circular Cylinder, 7.62cm dia. x7.62 cm ht. with longitudinal axis vertical	1.99	1.97		0.90	1.16	4.03	4.00
	1.60	1.41		0.83	0.64	2.88	2.67
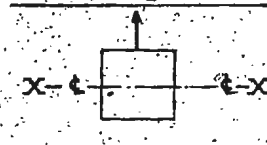 Rt.Circular Cylinder, 7.62cm dia, x7.62cm ht. with longitudinal axis horizontal	1.55	1.45	0.43	0.34	1.50	3.72	4.89
	1.11	1.14	0.32	0.32	1.02	2.80	3.34
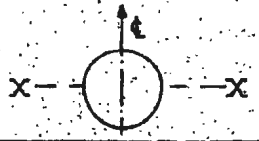 Sphere, 7.62 cm dia.	1.60	1.29	0.37		1.58	3.25	4.23
	1.08	0.99	0.37		1.04	2.40	2.89
 Hemisphere, 7.62 cm dia.	1.69	1.32	0.37		1.62	3.31	4.00
	1.15	1.00	0.37		1.10	2.47	2.67

* See Fig. 34 for the forces to be considered in the breakout of fully embedded objects and Appendix 'A' for sample calculation.

** X-X is embedment level.

CHAPTER V

CONCLUSIONS

Laboratory experiments were conducted to determine the adhesion and breakout resistance of soft underconsolidated clayey sediments. Plate models of different materials and roughness were used. Prismatic models and objects of various shapes were tested with partial and complete embedment.

1. Although the pull out resistance is generally attributed to the soil-object adhesion, the surface undulation could increase the resistance as demonstrated in the case of plexiglas sheets. Pull out resistance in such a case would be due to the shear between the soil surfaces.

2. In the cases where the breakout resistance is due to the adhesion between soil and object, the surface roughness directly influences the adhesion ratio.

3. Physico-chemical action such as that demonstrated for glass plate, would increase the soil-object bond and consequently the pull out resistance.

4. In the case of artificially sedimented soil, the period of primary sedimentation appears to have the greatest significance on the value of the adhesion ratio. The sedimentation time, in turn, affects the soil density,

liquidity index and its strength.

At very low soil strengths, the adhesion ratio α is very small in the order of 0.3. However, the value of α reaches a nearly constant value as the soil gains strength. From the tests conducted, beyond a value of 50 Pa of soil cohesion, the adhesion ratio reaches a value that is generally recommended even for terrestrial soils.

5. Tests on ice sheets are to be considered only partially successful. Pitting of the ice sheet is one of the experimental problems. For the range of shear strengths tested the value of the adhesion ratio appears to be nearly constant. The effects of the addition of antifreeze was not fully examined. Ice sheet experiments are to be considered superficial and deficient in detailed studies.

6. In the case of partially embedded objects, the base suction depends on the horizontal projected area of the base, regardless of its configuration. An exception, however, is the case of objects with dished bottom. For such objects the base suction increases because of soil to soil resistance, as proved by the experiments with a skirted base.

7. For fully embedded objects, the soil overburden causes an additional resistance. However, theoretical equations and shallow anchor uplift theories appear to over-estimate the breakout force in weak soils.

5.1 Limitations of the Present Investigation and Suggestions for Further Work

Generally, experiments with artificially sedimented soils are time consuming in terms of the period allowed for sedimentation. Within this constraint, some 91 test results are reported in this thesis (Appendix B) and discussed. Work of this type therefore forms part of an ongoing program. For the particular type of soil used, experiments with all materials were satisfactory and repeatable. There were, however, problems in the tests with ice sheets. Concerted efforts in the laboratory as well as in the ocean environment are recommended as a part of further research programs on ice-soil adhesion studies.

A wider range of material surface roughness is possible and so is the range of soil strength. Subject to time constraints, future tests in these directions are also recommended.

The effect of physico-chemical phenomenon is by itself a separate area of research. While there are a number of publications in this area, the adhesion aspect does not appear to have been examined in great detail. This is a potential area for further research.

Laboratory investigations by themselves are not the final answer to any engineering problem, particularly those related to soil mechanics. Large scale or full scale tests

are recommended at an appropriate stage to confirm the laboratory results.

REFERENCES

1. BYRNE, P.M. and FINN, W.D.L. 1978. Breakout of submerged structures buried to a shallow depth. Canadian Geotechnical Journal, 15 (2), pp. 146-154.

2. CHARI, T.R., GUHA, S.N., and MUTHUKRISHNAIAH, K. 1978. Adhesive resistance of underconsolidated sediments. Oceans '78, Washington, D.C., pp. 497-502.

3. CRC HANDBOOK ON MATERIALS SCIENCE. 1974. Vol. I, CRC Press Inc., Ohio, U.S.A., p. 333.

4. CSA STANDARD B95-1962. Surface Texture (Roughness, Waviness, and Lay). Canadian Standards Association, Ottawa, Canada.

5. DAVIE, J.R. and SUTHERLAND, H.B. 1977. Uplift resistance of cohesive soils. ASCE Journal of Geotechnical Engineering Division, 103 (GT9), pp. 935-952.

6. --------. 1978. Modeling of clay uplift resistance. ASCE Journal of Geotechnical Engineering Division, Technical Note, 104 (GT6), pp. 755-760.

7. DAVIE, J.R., FENSKE, C.W. and SEROCKI, S.T. 1978. Geotechnical properties of deep continental margin soils. Marine Geotechnology, 3 (1), pp. 85-122.

8. ERCHUL, R.A. and SMITH, R.J. 1969. Lubricant and Polymer reduction of sediment adhesion. ASCE Conference: Civil Engineering in the Oceans II, pp. 621-640.

9. FISK, H.N. and McCLELLAND, B. 1959. Geology of continental shelf off Louisiana: its influence on offshore foundation design. Geological Society of America Bulletin, Vol. 70, pp. 1369-1394.

10. FOCHT, J.A., Jr., and KRAFT, M., Jr. 1977. Progress in Marine Geotechnical Engineering. ASCE Journal of Geotechnical Engineering Division, 103 (GT10), pp. 1097-1118.

11. GIBSON, R.E. 1958. The progress of consolidation in a clay layer increasing in thickness with time. Geotechnique, Vol. 8, pp. 171-182.

12. GRIM, R.E. 1968. Clay Mineralogy. McGraw-Hill Book Company, New York.

13. HANNA, T.H. 1973. The influence of anchor inclination on pull out resistance of clays. Canadian Geotechnical Journal, 10(4), pp. 664-669.

14. HANSEN, J.B. 1961. A general formula for bearing capacity. Ingeniøren-International Edition, 5(2), pp. 38-46.

15. HELWICK, S.J., Jr., and BRYANT, W.R. 1977. Geology and Geotechnical characteristics of sediments in East Bay area, Mississippi Delta. Marine Geotechnology, Vol. 2, pp. 161-176.

16. JUDSON, S. 1968. Erosion of the land. American Scientist, 56(4), pp. 356-374.

17. KELLER, G.H. 1967. Shear strength and other physical properties of sediments from some ocean basins. ASCE Conference: Civil Engineering in the Oceans, pp. 391-417.

18. LEE, H.J. 1972. Unaided breakout of partially embedded objects from cohesive seafloor soils. Technical Report R-755, Naval Civil Engineering Laboratory, Port Hueneme, California.

19. LITTLETON, I. 1976. An experimental study of adhesion. Journal of Terramechanics, 13(3), pp. 141-152.

20. LIU, C.L. 1969. Ocean sediment holding strength against breakout of embedded objects. Technical Report R-635, Naval Civil Engineering Laboratory, Port Hueneme, California.

21. McCLELLAND, B. 1967. Progress of consolidation in delta front and prodelta clays of the Mississippi River. Marine Geotechnique, University of Illinois Press, Urbana, pp. 22-40.

22. MEYERHOF, G.G. and ADAMS, J.I. 1968. The ultimate uplift capacity of foundations. Canadian Geotechnical Journal, 5(1), pp. 225-244.

23. MEYERHOF, G.G. and MURDOCK, L.J. 1953. Bearing Capacity of piles in London clay. Geotechnique, 3, pp. 267-282.

24. MITCHELL, J.K. 1976. Fundamentals of soil behavior. John Wiley and Sons, Inc., New York.

25. MUGA, B.J. 1966. Breakout forces. Technical Note N-863, Naval Civil Engineering Laboratory, Port Hueneme, California.

26. ---------. 1968. Ocean bottom breakout forces, including field test data and development of an analytical method. Technical Report R-591, Naval Civil Engineering Laboratory, Port Hueneme, California.

27. NOORANY, I. and GIZIENSKI, S.F. 1970. Engineering properties of submarine soils: State-of-the-art Review. ASCE Journal of Soil Mechanics and Foundations Division, 96 (SM5), pp. 1735-1762.

28. OLSSON, R.G. 1949. Rigorous solution of a differential equation in Soil Mechanics. Quarterly Journal of Applied Mathematics, 7(3), pp. 228-342.

29. ---------. 1958. Approximate solution of the progress of consolidation in a sediment. Third International Conference on Soil Mechanics and Foundation Engineering, Zurich, Vol. 1, pp. 38-42.

30. POTYONDY, J.G. 1961. Skin friction between various soils and construction materials. Geotechnique, 11, pp. 339-353.

31. SANGREY, D.A. 1977. Marine Geotechnology - State of the art. Marine Geotechnology, Vol. 2, pp. 54-80.

32. SILVA, A.J., HOLLISTER, C.D., LAINE, E.P. and BEVERLY, B.E. 1976. Geotechnical properties of Deep sea sediments: Bermuda Rise. Marine Geotechnology, 1 (3), pp. 195-232.

33. TERZAGHI, K. 1956. Varieties of submarine slope failures. 8th Texas Conference on Soil Mechanics and Foundation Engineering, pp. 1-41.

34. TERZAGHI, K. and BECK, R.B. 1967. Soil Mechanics in Engineering Practice. John Wiley & Sons, Inc., New York.

35. TROLLOPE, D.H. 1960. The Fabric of clays in relation to shear strength. 3rd. Proceedings, Australia-New Zealand Conference on Soil Mechanics and Foundation Engineering, pp. 197-202.

36. VESIC, A.S. 1971. Breakout resistance of objects embedded in ocean bottom. ASCE Journal of Soil Mechanics and Foundations Division, 97(SM9), pp. 1183-1205.

37. --------. 1973. Analysis of ultimate loads of shallow foundations. ASCE Journal of Soil Mechanics and Foundations Division, 99 (SM1), pp. 45-73.

38. VESIC, A.S. and BARKSDALE, R.D. 1963. Theoretical studies and cratering mechanisms affecting the stability of cratered slopes. Final Report, Project No. A-655, Engineering Experiment Station, Georgia Institute of Technology, Atlanta, Ga., p. 103.

39. VESIC, A.S., BOUTWELL, G.P., Jr., and TAI, T.L. 1965. Engineering properties of nuclear craters. Technical Report No. 3-699, Report 2, U.S. Army Engineers Waterways Experiment Station, Vicksburg, Miss., p. 123.

40. WANG, M.C., DEMARS, K.R. and NACCI, V.A. 1977. Breakout capacity of model suction anchors in soil. Canadian Geotechhical Journal, 14(2), pp. 246-257.

41. WITNEY, B.D. 1968. The determination of soil particle movement in two-dimensional failure. Journal of Terramechanics, 5(1), pp. 39-52.

APPENDIX A

SAMPLE CALCULATION FOR BREAKOUT RESISTANCE OF FULLY EMBEDDED SPHERICAL OBJECT

Derivation of expression for breakout resistance

The breakout load for fully embedded spherical objects comprises three resistive forces as given below.

1. Base suction
2. Vertical component of adhesion along top curved surface
3. Shearing resistance along assumed soil failure plane above the embedded object.

Base suction: The base suction over unit area was calculated from eq. [8] and the total base suction (P_s) was computed by multiplying the unit base suction, p_s, with the projected area of the base, A_b. β used in eq. [8] was obtained from Figure 32 for corresponding D/B value.

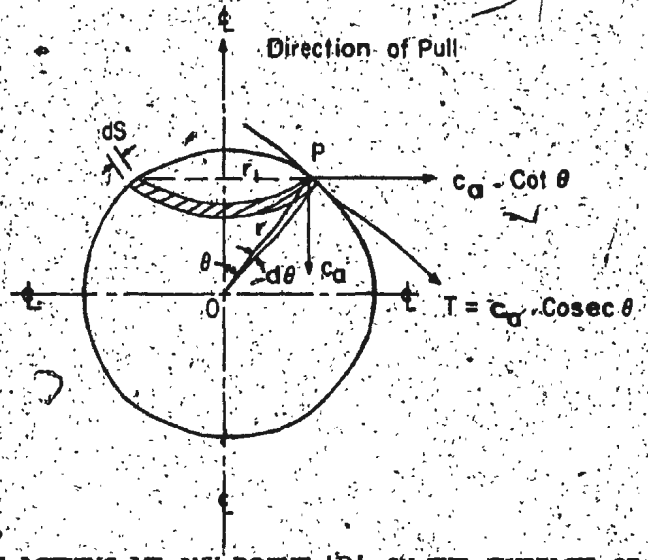

Fig. A-1 FORCES ACTING AT ANY POINT 'P' ON THE SURFACE OF A SPHERE AT THE ONSET OF BREAKOUT

Adhesion on top curved surface: The forces acting at any point P(r, θ) on the surface of the sphere at the onset of breakout are shown in Figure A-1, where

T = adhesive force acting along the tangent at point P

c_a = vertical component of force, T

c_a . Cot θ = horizontal component of force, T.

The summation of the horizontal components of T over the top hemispherical surface is zero, whereas the summation of the vertical components gives the effective adhesion, and is computed as follows:

Effective adhesion on an elemental disc at point P

$= c_a . [2\pi r_1 . ds]$, r_1 = radius of the elemental disc

$= c_a [2\pi r \text{ Sin } \theta . r d\theta]$, r = radius of the sphere

$= c_a . 2\pi r^2 \text{ Sin } \theta . d\theta$

Integrating over the whole hemispherical surface,

total vertical component of adhesion, $C_{ta} = \int_0^{\pi/2} c_a 2\pi r^2 \sin\theta . d\theta$

$= c_a . 2\pi r^2 [-\cos\theta]_0^{\pi/2}$

$= c_a . 2\pi r^2$

Sample calculation

D = 8.25 cm

B = 7.62 cm

$\therefore \frac{D}{B} = 1.08$, giving $\beta = 4.1$ from Figure 32

$\bar{c} = 52.76$ Pa, the average of the cohesion values shown in Figure A-2

$c_b = 52.76$ Pa

Base suction, $P_s = \beta . c_b . A_b$

$= (4.1)(52.76) . \frac{\pi (7.62)^2}{(4)(10,000)}$

$= 0.99$ N

Vertical component of adhesion, $C_{ta} = c_a . 2\pi r^2$
(on top curved surface)

$= (52.76) . (2) \frac{\pi (3.81)^2}{10,000}$

$= 0.37$ N

Shearing resistance, $C_{AB} = \bar{c} . 2\pi r . AB$

$= (52.76)(2)\pi \frac{(3.81)(8.25)}{10,000}$

$= 1.04$ N

Hence,

total breakout load, $B = P_s + C_{ta} + C_{AB}$

$= 0.99 + 0.37 + 1.04$

$= 2.40$ N

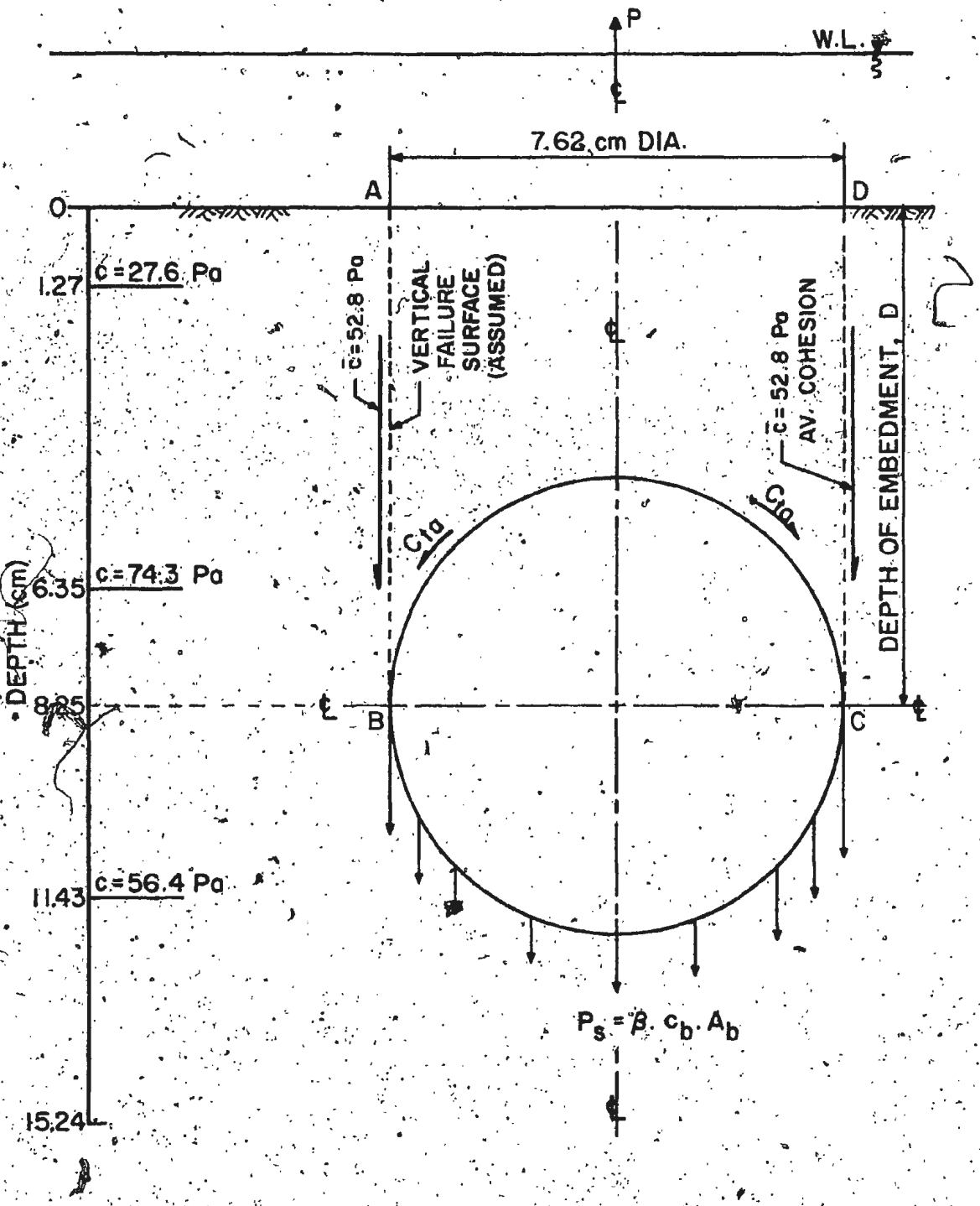

Fig. A-2 FORCES ACTING ON A FULLY EMBEDDED SPHERICAL OBJECT AT THE ONSET OF BREAKOUT

APPENDIX B

SUMMARY OF LABORATORY EXPERIMENTS CONDUCTED

Category	Type and Size of Object	Type of Material and Roughness Values over 0.254 mm Cut-off Length (μm)	Type of Embedment	$\frac{D}{B}$ Ratio	Period of Sedimentation (Hours)	Objectives
1	2	3	4	5	6	7
I	Flat Plate (25 cm x 15 cm)	Glass (0.00762)	Partial	N.A.	2, 10, 16, 24, 48, 72	Adhesive Resistance of Very Soft Clay on Materials of Different Roughnesses
		Plexiglas (0.03048)	Partial	N.A.	2, 8, 10, 12, 16, 24, 48, 72	
		Brass (0.04445)	Partial	N.A.	2, 10, 16, 24, 48, 72	
		Mild Steel, Painted (0.1778)	Partial	N.A.	2, 10, 16, 24, 48, 72	
		Stainless Steel (0.1905)	Partial	N.A.	2, 10, 16, 24, 48, 72	
		Mild Steel, Rusted - II (2.195)	Partial	N.A.	2, 10, 16, 24, 48, 72	
		Mild Steel Rusted - I (3.937)	Partial	N.A.	2, 10, 16, 24, 48, 72	
		Ice Sheet	Partial	N.A.	2, 10, 16, 24, 48, 72	

SUMMARY OF LABORATORY EXPERIMENTS CONDUCTED (cont'd.)

Category	Type and Size of Object	Type of Material and Roughness Values over 0.254 mm Cut-off Length (μm)	Type of Embedment	$\frac{D}{B}$ Ratio	Period of Sedimentation (Hours)	Objectives
1	2	3	4	5	6	7
II	Square Prism (7.92 cm Side) with Flat Base	Plexiglas (0.03048)	Partial	1.79	2, 10, 16, 24, 48, 72	Determination of 'Base Suction' and the Influence of Base Configuration on 'Base Suction'
				0	48	
				1.55	48	
				2.70	48	
				4.02	48	
				6.13	48	
	Square Prism (7.92 cm Side) with Pyramidal Base, Apex Angle 90°	Plexiglas (")	Partial	1.79	2, 10, 16, 24, 48, 72	
				1.70	48	
	Square Prism (7.92 cm Side) with Pyramidal Base, Apex Angle 135°	Plexiglas (")	Partial	1.92	2, 10, 16, 24, 48, 72	
				1.99	48	
	Square Prism (7.92 cm Side) with All Round Skirt, 5 cm deep	Plexiglas (")	Partial	1.60	2, 10, 16, 24, 48, 72	

SUMMARY OF LABORATORY EXPERIMENTS CONDUCTED (cont'd.)

Category	Type and Size of Object	Type of Material and Roughness Values over 0.254 mm Cut-off Length (μm)	Type of Embedment	$\frac{D}{B}$ Ratio	Period of Sedimentation (Hours)	Objectives
1	2	3	4	5	6	7
III	Cube (7.92 cm Side)	Plexiglas (0.03048)	Full	1.5	48	Breakout Resistance
				2.0	48	
	Right Circular Cylinder (7.62 cm dia. x 7.62 cm ht.) with Longitudinal Axis Vertical	Plexiglas (")	Full	1.6	48	
				2.0	48	
	Right Circular Cylinder (7.62 cm dia. x 7.62 cm ht.) with Longitudinal Axis Horizontal	Plexiglas (")	Full	1.1	48	
				1.6	48	
	Sphere (7.62 cm dia.)	Plexiglas (")	Full	1.1	48	
				1.6	48	
	Hemisphere (7.62 cm dia.) with Flat Base Horizontal	Plexiglas (")	Full	1.2	48	
				1.7	48	